STEM CELLS

USP7 represses lineage differentiation genes in mouse embryonic stem cells by both catalytic and noncatalytic activities

Chao Liu[1,2]†, Lingang Sun[1]†, Yijun Tan[1], Qi Wang[1], Tao Luo[1], Chenlu Li[1], Nan Yao[3,4,5], Yuting Xie[3,4,5], Xiao Yi[3,4,5], Yi Zhu[3,4,5], Tiannan Guo[3,4,5], Junfeng Ji[1,6,7,8]*

USP7, a ubiquitin-specific peptidase (USP), plays an important role in many cellular processes through its catalytic deubiquitination of various substrates. However, its nuclear function that shapes the transcriptional network in mouse embryonic stem cells (mESCs) remains poorly understood. We report that USP7 maintains mESC identity through both catalytic activity–dependent and –independent repression of lineage differentiation genes. *Usp7* depletion attenuates SOX2 levels and derepresses lineage differentiation genes thereby compromising mESC pluripotency. Mechanistically, USP7 deubiquitinates and stabilizes SOX2 to repress mesoendodermal (ME) lineage genes. Moreover, USP7 assembles into RYBP-variant Polycomb repressive complex 1 and contributes to Polycomb chromatin–mediated repression of ME lineage genes in a catalytic activity–dependent manner. USP7 deficiency in its deubiquitination function is able to maintain RYBP binding to chromatin for repressing primitive endoderm–associated genes. Our study demonstrates that USP7 harbors both catalytic and noncatalytic activities to repress different lineage differentiation genes, thereby revealing a previously unrecognized role in controlling gene expression for maintaining mESC identity.

INTRODUCTION

The pluripotent transcriptional network in mouse embryonic stem cells (mESCs) is controlled by the interplay between DNA binding transcription factors (TFs) and chromatin regulators (*1*, *2*). Master TFs including OCT4, SOX2, and NANOG (OSN) establish a core transcriptional regulatory circuitry by activating pluripotency-associated gene transcription and repressing lineage differentiation genes and therefore are essential to the maintenance of mESC identity (*3*, *4*). Individual OSN collectively maintains a balanced pluripotency state by driving specification into a particular lineage while inhibiting alternative differentiation trajectories in a mutually exclusive manner (*3*). For example, SOX2 specifies mESCs into ectoderm (ECT) and inhibits a group of mesoendodermal (ME) genes such as *T*, *Hand1*, etc., but on the contrary, OCT4 acts as an ME lineage specifier and prohibits ECT development (*5*, *6*). The inhibition of lineage differentiation transcription program by OSN largely relies on their interplay with repressive chromatin regulators such as Polycomb group (PcG) proteins (*4*, *7*).

PcG proteins assemble into Polycomb repressive complex 1 (PRC1) and PRC2 that silence developmental genes through inhibitory histone modifications (*8*, *9*). PRC2 catalyzes methylation of histone H3 at lysine-27 (H3K27me3) (*10*). PRC1 monoubiquitylates histone H2A at lysine-119 (H2AK119ub1) through E3 ligases RING1A and RING1B, which, together with one of the six PcG RING finger proteins (PCGF1 to PCGF6), form six subcomplexes (PRC1.1 to PRC1.6) (*11*). While PRC1.2 and PRC1.4 belong to canonical PRC1, the rest (PRC1.1, PRC1.3, PRC1.5, and PRC1.6) are variant PRC1 (vPRC1), which contains RYBP/YAF2 together with various accessory proteins (*9*, *11*). A series of feedback and communication mechanisms underpin the formation of repressive PRC2-H3K27me3 and PRC1-H2AK119ub1 chromatin domain that is thought to repress transcription by restricting access of transcriptional regulators to gene promoters (*8*, *9*, *12*). Catalytic activity of RING1B in vPRC1 is shown to be essential to Polycomb-mediated gene repression in mESCs through H2AK119ub1 deposition (*13*, *14*). Among vPRC1 complexes, PRC1.1 comprising BCOR, KDM2B, ubiquitin (Ub)–specific peptidase 7 (USP7), and SKP1 accessory proteins in addition to RING1B, RYBP, and PCGF1 is responsible for repressing the largest number of genes in mESCs (*15*, *16*). However, how PRC1.1 subunits such as USP7, a deubiquitinase (DUB) that regulates posttranslational ubiquitination of both histone and nonhistone proteins (*17*), shape the transcriptional network in mESCs remains unclear.

In this study, we show that USP7 depletion leads to loss of pluripotency characterized by reduced level of SOX2 concomitant with derepression of lineage differentiation genes. USP7 deubiquitinates and maintains SOX2. Moreover, USP7 assembles as a subunit of RYBP-vPRC1 and contributes to H2AK119ub1-mediated repression of ME lineage genes dependently of its catalytic activity. USP7 is capable of maintaining RYBP binding on chromatin to repress primitive endoderm (PE)–associated genes in a catalytic activity–independent manner. Overall, our study provides previously

[1]Center of Stem Cell and Regenerative Medicine, and Bone Marrow Transplantation Center of the First Affiliated Hospital, Zhejiang University School of Medicine, Hangzhou 310058, China. [2]Zhejiang University-University of Edinburgh Institute, Zhejiang University School of Medicine, Haining 314400, China. [3]Westlake Laboratory of Life Sciences and Biomedicine, Key Laboratory of Structural Biology of Zhejiang Province, School of Life Sciences, Westlake University, Hangzhou 310030, China. [4]Center for Infectious Disease Research, Hangzhou 310030, China. [5]Institute of Basic Medical Sciences, Westlake Institute for Advanced Study, Hangzhou 310030, China. [6]Zhejiang Engineering Laboratory for Stem Cell and Immunotherapy, Institute of Hematology, Zhejiang University, Hangzhou 310058, China. [7]Department of Geriatrics, Affiliated Hangzhou First People's Hospital, Zhejiang University School of Medicine, Hangzhou 310006, China. [8]Eye Center, The 2nd Affiliated Hospital, School of Medicine, Zhejiang University, Zhejiang Provincial Key Laboratory of Ophthalmology, Zhejiang Provincial Clinical Research Center for Eye Diseases, Zhejiang Provincial Engineering Institute on Eye Diseases, Hangzhou, Zhejiang 310009, China.
*Corresponding author. Email: jijunfeng@zju.edu.cn
†These authors contributed equally to this work.

unidentified evidence that USP7 maintains mESC identity through both catalytic activity and noncatalytic structural function to repress lineage differentiation genes.

RESULTS

USP7 is highly expressed in mouse pluripotent cells

To investigate the genes encoding USP family proteins that are highly expressed in mouse pluripotent cells, we first analyzed the published gene expression data of mESCs and mouse embryonic fibroblasts (MEFs) (*18*). We found that there are 19 USP-coding genes including *Usp1*, *Usp7*, *Usp21*, and *Usp44* that are highly expressed in mESCs compared to MEFs (Fig. 1A), suggesting that they may play a role in the maintenance of mESCs. Among the list, USP21 has been shown to deubiquitinate NANOG to maintain mESCs (*19*–*21*), and USP44 down-regulation is required for neural differentiation of mESCs by regulating monoubiquitination of histone H2B on lysine-120 (H2Bub1) (*22*). Since USP7 is also involved in PRC1.1 (*9*, *11*), we also analyzed the expression of PRC1.1 subunit–coding genes in mESCs and MEFs. Similar to *Rybp* and *Kdm2b* that have been previously reported to maintain mESCs (*23*–*26*), *Usp7* was found to be more enriched in mESCs relative to MEFs (Fig. 1B). To validate the enriched expression of USP7 in mESCs, we then examined the protein expression of USP7 in MEFs, undifferentiated mESCs, and differentiated mESCs induced by leukemia inhibition factor (LIF) withdrawal. Our results confirmed that USP7, similar to OSN, was highly expressed in mESCs relative to MEFs and the expression level declined during LIF withdrawal–induced differentiation (Fig. 1C). Similarly, the expression of USP7 declined together with OSN during differentiation of mESCs induced by retinoic acid (RA) (Fig. 1D). We also found that USP7 was abundantly expressed in human pluripotent stem cells including human embryonic stem cells (hESCs) and induced pluripotent stem cells (hiPSCs) as opposed to human foreskin fibroblasts (HFFs) (fig. S1A). To further look into *Usp7* expression in lineages during early mouse embryonic development, we performed immunostaining of USP7 in mouse E3.5 (embryonic day 3.5) blastocyst embryos, and our results showed that USP7 expression appeared to be enriched in, although not restricted to, inner cell mass (ICM) (fig. S1B). Furthermore, we analyzed the published single-cell gene expression data of early mouse embryo (*27*). Correlation analysis of *Usp7* with pluripotency, PE, and trophectoderm (TE) lineage markers expression in ICM during mouse embryonic development showed that the expression of *Usp7* and *Sox2* was well correlated (Fig. 1E). Our analyzed results showed that, similar to *Sox2* and *Pou5f1*, *Usp7* was more notably restricted to ICM than TE lineage at late 32–cell stage mouse embryos (Fig. 1, F to I, and fig. S1C). Moreover, we also examined the expression of USP7 together with other pluripotency-related genes at both RNA and/or protein levels in naïve mESCs cultured in "2i" inhibitor cocktail comprising mitogen-activated protein kinase kinase and glycogen synthase kinase 3 inhibitors plus LIF (2i/LIF) versus LIF/serum conditions (*28*). By analyzing the published RNA sequencing (RNA-seq) data (*29*), we found that *Usp7*, *Sox2*, and *Pou5f1* appeared to be more enriched in mESCs cultured under LIF/serum condition (fig. S1D), which was also verified by our quantitative polymerase chain reaction (qPCR) results (fig. S1E). Our immunoblotting data showed that, unlike NANOG known to be more highly expressed in naïve mESCs (*28*), USP7, SOX2, and OCT4 were expressed at similar protein levels under both 2i/LIF and LIF/serum conditions (fig. S1F). It suggests that there could be posttranscriptional/translational mechanisms to regulate *Usp7* expression in different pluripotent states of mESCs. Together, our results demonstrated that USP7 is enriched in pluripotent cells, suggesting that it may be involved in the maintenance of pluripotency.

USP7 is required to maintain mESC identity

In an attempt to assess the functional role of USP7 in regulating mESCs, we first performed lentiviral short hairpin RNA (shRNA)–based gene silencing approach using three independent shRNAs targeting *Usp7* (sh*Usp7*#1, sh*Usp7*#2, and sh*Usp7*#3) and a scrambled negative control (shCtrl). Albeit with varied efficiency, sh*Usp7*#1, sh*Usp7*#2, or sh*Usp7*#3 all significantly suppressed *Usp7* expression in mESCs at 7 days after infection (fig. S2A). Therefore, the samples at day 7 after infection were selected for further experiments. We observed that knockdown of *Usp7* expression robustly inhibited the growth of mESCs (Fig. 2A), which is likely attributed to its known role in regulating MDM2-p53 axis (*30*). Our immunoblotting results showed that while *Usp7* knockdown decreased MDM2 level, it did not lead to increased p53 level (fig. S3A), suggesting that USP7 regulates both MDM2 and p53 in mESCs. Growth curve and cell cycle analyses also confirmed that *Usp7* knockdown significantly impaired the proliferation of mESCs (fig. S3, B and C), consistent with its known role in regulating DNA replication (*31*). Nevertheless, in line with p53 result (fig. S3A), we did not observe significant changes in apoptosis by *Usp7* knockdown (fig. S3D).

Moreover, *Usp7* depletion also induced a changed morphology of mESC colonies suggestive of spontaneous differentiation, suggesting that it plays a role in maintaining the undifferentiated state of mESCs (Fig. 2A). *Usp7* suppression did not lead to significant changes in the transcript levels of pluripotency-associated factors such as *Pou5f1*, *Sox2*, *Nanog*, and *Klf4* at different days of infection as shown by gene expression analysis (Fig. 2B and fig. S2, C and D). However, immunoblotting analysis revealed that *Usp7* depletion robustly decreased the protein level of SOX2 together with RING1B, its known PRC1-related substrate (*32*), whereas it had no obvious impact on OCT4, NANOG, RYBP, and H2AK119ub1 levels (Fig. 2C). The immunofluorescent staining analyses also confirmed that the *Usp7* suppression reduced SOX2, but not OCT4, signals in mESCs (fig. S2B). These results suggested that USP7 may posttranslationally regulate *Sox2* expression in mESCs. To further examine the function of USP7 to regulate self-renewal of mESCs, we performed colony formation assay. Our results showed that sh*Usp7*#1- and sh*Usp7*#2-mediated knockdown significantly decreased the colony-forming efficiency compared to shCtrl (Fig. 2D), demonstrating that USP7 is required for the self-renewal of mESCs. We next performed teratoma assay to evaluate the pluripotency of mESCs after *Usp7* depletion. Since sh*Usp7*#2 exhibited the best knockdown performance (fig. S2A), we subcutaneously injected the sh*Usp7*#2-depleted or shCtrl-infected mESCs into Balb/c nude mice. We found that the volumes of tumors formed by sh*Usp7*#2-depleted mESCs were significantly smaller than that generated by shCtrl-infected mESCs at 5 weeks after injection (Fig. 2E). Furthermore, the histological analysis showed that although tumors derived from sh*Usp7*#2-depleted mESCs exhibited comparable muscle tissue representative of mesoderm to that generated from shCtrl-infected mESCs, abnormal glandular structure

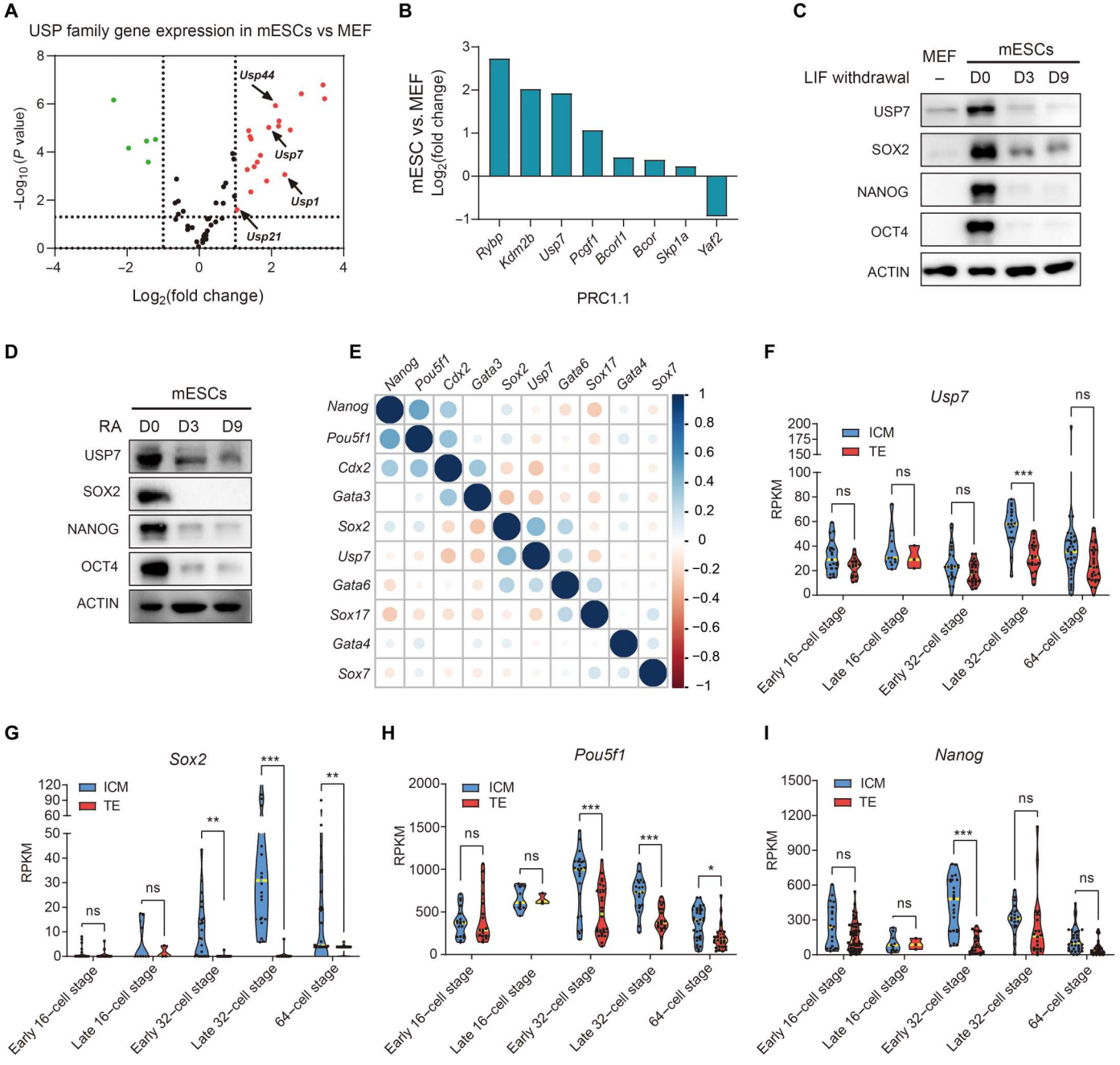

Fig. 1. USP7 is highly expressed in mouse pluripotent cells. (**A**) *Usp* family gene expression in mESCs versus MEFs by analysis of previously published data (*27*). (**B**) PRC1.1 gene expression in mESCs versus MEFs by analysis of previously published data (*27*). (**C**) Immunoblotting of USP7 and OSN at days 0, 3, and 9 of differentiation induced by withdrawal LIF. ACTIN serves as the loading control. (**D**) Immunoblotting of USP7 and OSN at days 0, 3, and 9 RA-induced differentiation. ACTIN serves as the loading control. (**E**) Corrplot showed the correlation analysis of *Usp7*, *Pou5f1*, *Sox2*, *Nanog*, PE, and TE lineage marker expression in ICM of 32–cell stage mouse embryos (*27*). (**F** to **I**) The expression of *Usp7*, *Sox2*, *Pou5f1*, and *Nanog* in ICM and TE lineages by analyzing the published single-cell RNA-seq data during early mouse embryonic development (*27*). ns, not significant. **P* < 0.05; ***P* < 0.01; ****P* < 0.001.

and keratinocytes in epidermis representative of endoderm and ECT, respectively, were observed in sh*Usp7*#2-depleted group (Fig. 2F). Therefore, our results suggest that knockdown of *Usp7* compromised teratoma formation ability of mESCs and support that USP7 is required for the pluripotency maintenance of mESCs. To look into how USP7 regulates gene expression, we did RNA-seq for shCtrl- and sh*Usp7*#2-infected mESCs. We found that USP7 depletion up-regulated and down-regulated genes largely enriched in tissue/embryonic morphogenesis/cell fate commitment and metabolic process (fig. S2, G to I, and table S3), respectively. These results suggest that USP7 represses lineage differentiation genes and maintains cell metabolism–associated genes in mESCs.

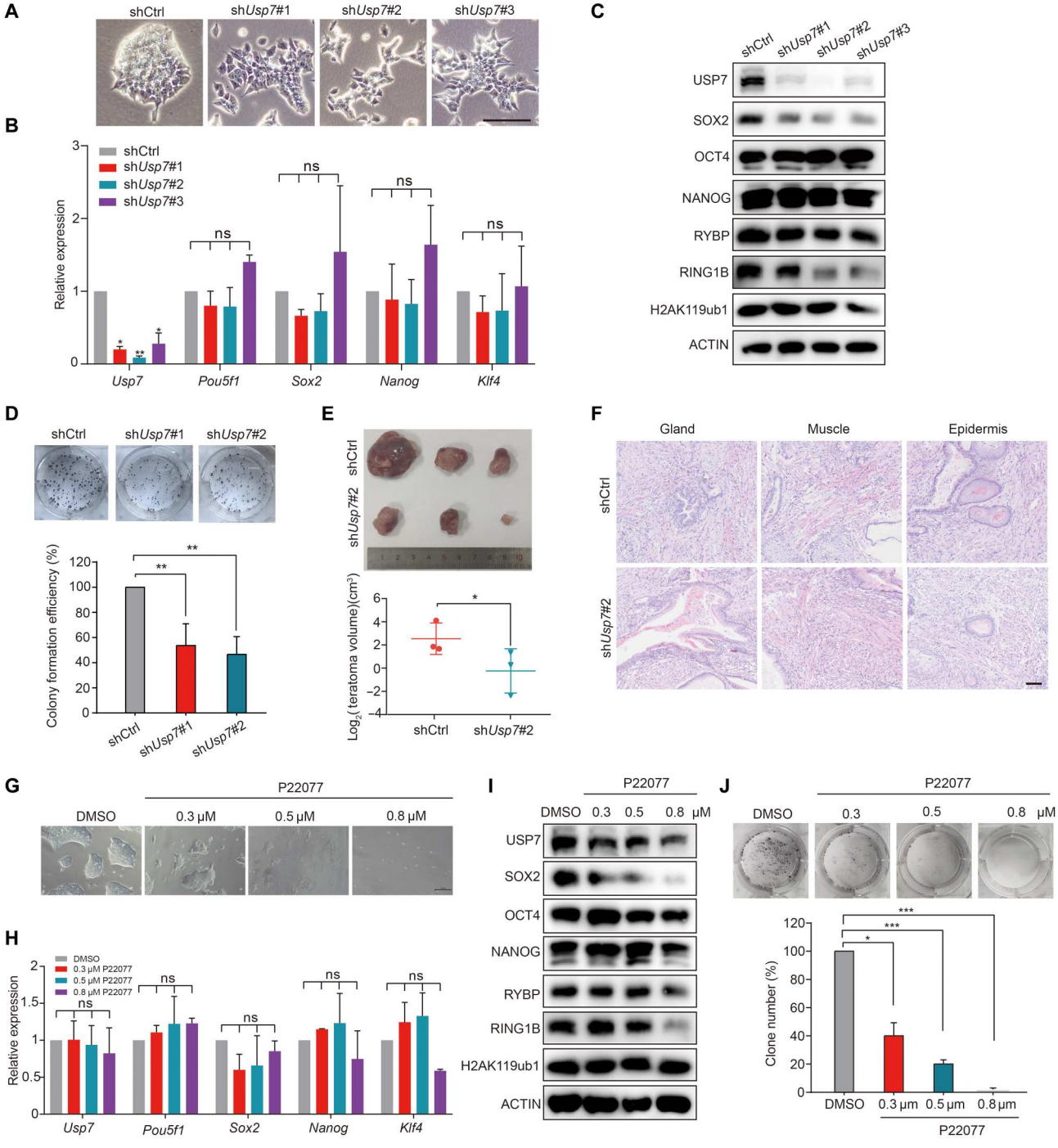

Fig. 2. USP7 is required for the maintenance of mESCs. (**A**) Morphology of mESCs 7 days after infections with shCtrl and three sh*Usp7*. Scale bar, 50 μm. (**B**) Reverse transcription (RT) qPCR analysis of *Usp7*, *Pou5f1*, *Sox2*, *Nanog*, and *Klf4* genes at day 7 after infection of mESCs with shCtrl and sh*Usp7*. Biological replicates, $n = 3$. $^{*}P < 0.05$; $^{**}P < 0.01$. (**C**) Immunoblotting of USP7, OSN, PRC1 subunits, and H2AK119ub1 in mESCs 5 days after infection with shCtrl and sh*Usp7*. (**D**) Colony-forming efficiency of mESCs 7 days after infection with shCtrl and sh*Usp7* based on alkaline phosphatase staining. Percentages were normalized to the shCtrl. Biological replicates, $n = 3$; two-tailed Student's *t* tests, $^{**}P < 0.01$. (**E**) Analysis of tumor sizes about 5 weeks after subcutaneous injection of shCtrl- and sh*Usp7*-infected mESCs into Balb/c nude mice. Three nude mice were injected for each group. Two-tailed *t* tests were used ($^{*}P < 0.05$). (**F**) Representative histological images of the tumors in (E) showing gland, muscle, and epidermis tissues, respectively. Scale bar, 50 μm. (**G**) Morphology of mESCs after 7 days of treatment with dimethyl sulfoxide (DMSO) or P22077. Scale bar, 100 μm. (**H**) RT-qPCR analysis of *Usp7*, *Pou5f1*, *Sox2*, *Nanog*, and *Klf4* at day 7 after treatment of mESCs with DMSO or P22077. Biological replicates, $n = 3$. (**I**) Immunoblotting of USP7, OSN, and PRC1 subunits 5 days after treatment of mESCs with DMSO or P22077. (**J**) Colony-forming efficiency of mESCs 7 days after treatment with DMSO and P22077. Percentages were normalized to DMSO treatment. Biological replicates, $n = 3$; two-tailed Student's *t* tests, $^{*}P < 0.05$ and $^{***}P < 0.001$.

To further test the role of its catalytic activity in maintaining mESCs, we then treated mESCs with P22077, a known USP7 enzymatic inhibitor (*33*). Compared to the control, P22077 treatment suppressed the growth of mESCs in a concentration-dependent manner (Fig. 2G), likely due to the increased p53 level after USP7 inhibition (*30*). In support of this, our immunoblotting data showed that P22077 treatment, particularly at high concentration (0.8 μM), appeared to increase p53 level, which was likely a result of the reduced level of MDM2 caused by the inhibition of USP7 DUB activity (fig. S3E). Consistently, P22077 treatment significantly increased the percentage of mESCs undergoing apoptosis at the examined concentrations (fig. S3F). It suggests that P22077 treatment appears more robust to inhibit the enzymatic activity of USP7. Similar to our shRNA-mediated knockdown results, P22077 treatment also robustly reduced SOX2 and RING1B protein levels without affecting the transcript levels of pluripotency-related genes (Fig. 2, H and I, and fig. S2, E and F). Moreover, P22077 treatment also significantly reduced the colony-forming efficiency of mESCs and almost abolished colony formation at the concentration of 0.8 μM (Fig. 2J). Together, these results indicate that the enzymatic inhibitor of USP7 phenocopied the effect of sh*Usp7* depletion on mESCs, therefore suggesting that the catalytic activity of USP7 is indispensable for the self-renewal and pluripotency maintenance of mESCs.

USP7 interacts with SOX2 and vPRC1 subunits

To further look into the mechanisms by which USP7 maintains pluripotency, we first attempted to identify its interactome in the nucleus by immunoprecipitating USP7 or immunoglobulin G (IgG) control from the nuclear extracts of mESCs and then performing liquid chromatography–tandem mass spectrometry (LC-MS/MS) analysis in five well-correlated replicates (fig. S4A). Our MS experiments identified a total number of 3240 proteins that were significantly enriched in USP7 immunoprecipitation (IP) samples versus IgG control (table S4). Gene Ontology (GO) pathway analysis showed that USP7-interacting proteins were largely enriched in chromatin organization function (fig. S4B). Among its nuclear interacting partners were PcG proteins such as MGA, RNF2/RING1B, PCGF6, EZH1, and PCGF1, in addition to its known DUB substrate p53 (*30*), supporting that USP7 is engaged in PRC as previously reported (Fig. 3A and fig. S4C) (*11*). The protein-protein interaction (PPI) analysis of USP7 interactome classified its interacting proteins into distinct modules comprising PcG proteins, DNA replication, DNA damage/repair, cell death, and pluripotency regulation comprising core pluripotent TFs such as OCT4, SOX2, and NANOG (fig. S4C), suggesting that USP7 might exert its function via being involved in different regulatory protein modules. To look into this possibility, we performed glycerol gradient fractionation from mESC lysates, followed by immunoblotting. Our results showed that USP7 was mainly distributed in low– and intermediate–molecular weight fractions (fractions 11 to 18) (Fig. 3B). We found that in the low–molecular weight fractions (fractions 11 to 13), USP7 correlated with PRC1.1 subunits including RING1B, RYBP, and PCGF1 (Fig. 3B, red box), whereas USP7 cosegregated with SOX2, OCT4, and RYBP to some extent in the intermediate–molecular weight fractions (fractions 14 to 18) (Fig. 3B, blue box). Thus, it suggests that USP7 forms distinct protein complexes together with SOX2, OCT4, and RYBP as well as PRC1 components, respectively. We then moved on to verify this by performing IP experiments. Consistent with the MS results (fig. S4D), our IP results showed that endogenous USP7 was able to robustly precipitate SOX2 but only weakly pull down OCT4 and NANOG (Fig. 3C). Reversely, endogenous SOX2 could also immunoprecipitate USP7 in addition to its known interaction partner OCT4 (*34*), but not RING1B and RYBP (Fig. 3D), under high-salt condition. We then constructed and transfected Flag-USP7 and hemagglutinin (HA)–SOX2 plasmids into human embryonic kidney (HEK) 293T cells, and subsequent co-IP results confirmed the interaction between exogenous USP7 and SOX2 (Fig. 3E). Therefore, these results suggest that USP7 specifically interacts with SOX2 among the core pluripotent TFs in mESCs. Moreover, our IP results also showed that USP7 interacted with RING1B, RYBP, and PCGF1 (Fig. 3F). USP7 was also able to precipitate PCGF5 and, less robustly, PCGF3, suggesting that USP7 might be also involved in PRC1.3/5 regulation. To examine whether bridging chromatin is involved in the interaction of USP7 with SOX2, we pretreated nuclear extracts of mESCs with or without benzonase endonuclease to remove nucleic acids and then performed USP7 IP and immunoblotting of SOX2 and RING1B. Our results showed that benzonase pretreatment reduced, but did not abolish, the interaction of USP7 with SOX2, similar to RING1B, suggesting that DNA/chromatin contributes to but is unlikely entirely responsible for their interaction (Fig. 3G).

USP7 has been previously shown to consist of a tumor necrosis factor receptor–associated factor (TRAF) domain, a catalytic center and a Ub-like domain (Fig. 3H) (*35*). To further identify which domain of USP7 interacts with its partners, we generated USP7 wild-type (USP7WT), ΔTRAF (62 to 208 deletion) and ΔEnzy (208 to 560 deletion) truncates, and C224S or C224A point mutation that disrupts the core site of its DUB catalytic activity (homologous to C223 in human) tagged with Flag plasmids (Fig. 3H) (*32*, *36*). We transfected them or the control vector into mESCs and then performed IP, followed by immunoblotting. Our results showed that neither deletion of enzymatic domain nor catalytic site mutant (C224S) did impair the interaction of exogenous USP7 with SOX2, RING1B, and RYBP (Fig. 3I). However, absence of TRAF domain nearly abolished their interaction (Fig. 3I), indicating that TRAF domain is mainly responsible for the interaction of USP7 with those partners in mESCs.

USP7 deubiquitinates and stabilizes SOX2

Given that USP7 interacts and positively regulates SOX2 expression (Figs. 2 and 3), we further examined whether USP7 can stabilize SOX2 protein. We cotransfected Flag-C224S/A mutants or Flag-USP7WT in stable PiggyBac transposon overexpression construct with HA-SOX2 transient overexpression plasmid into HEK293T. Immunoblotting results showed that overexpression of Flag-USP7WT sustained the expression of HA-SOX2 5 days after transfection when it was nearly undetectable in the empty vector–transfected cells (Fig. 3J). By contrast, overexpression of Flag-C224S/A failed to maintain HA-SOX2 level (Fig. 3J). Furthermore, we examined SOX2 protein turnover at different time points in shCtrl-, sh*Usp7*#2-, and sh*Usp7*#3-infected mESCs after treatment with cycloheximide (CHX), an inhibitor of protein synthesis. Our results showed that *Usp7* knockdown significantly accelerated SOX2 protein turnover rate (Fig. 3K). Therefore, these results suggested that USP7 may stabilize SOX2 via its DUB catalytic activity.

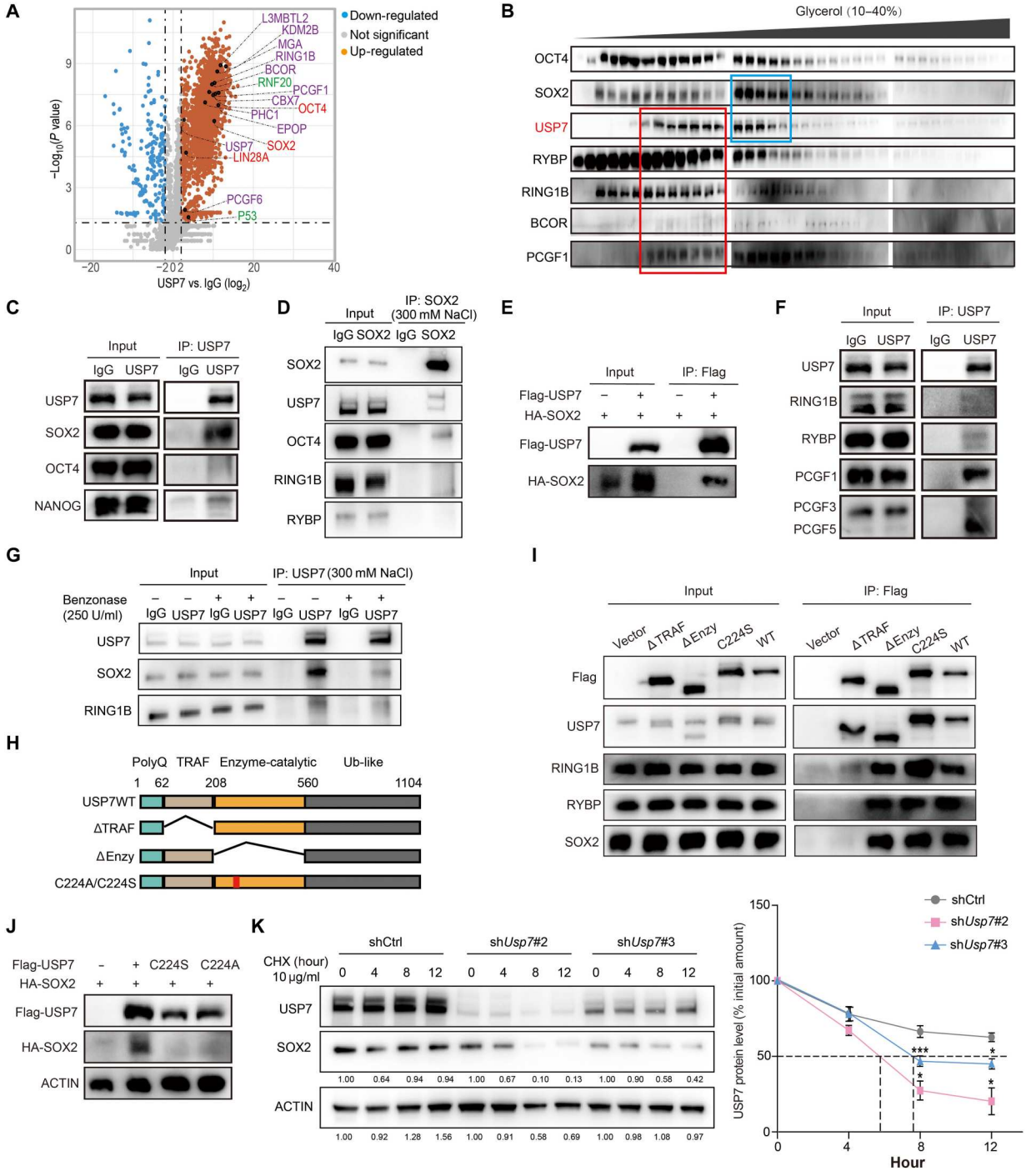

Fig. 3. USP7 interacts with SOX2 and PRC1 subunits. (**A**) The volcano plot showing representative proteins identified by MS and significantly associated with USP7 versus IgG in mESCs. Biological replicates, $n = 5$; Student's t test, $P < 0.05$. (**B**) Immunoblotting of mESC lysates fractionated on a glycerol gradient. Red and blue boxes indicate fractions containing PRC1 complex and most abundant SOX2 and USP7, respectively. (**C**) Endogenous IP of USP7 from nuclear extracts of mESCs followed by immunoblotting of USP7 and OSN. (**D**) Endogenous IP of SOX2 from nuclear extracts of mESCs followed by immunoblotting of SOX2, USP7, OCT4, RING1B, and RYBP. (**E**) Flag IP of nuclear extracts from HEK293T cells transfected with Flag-USP7 and HA-SOX2 followed by immunoblotting of Flag and HA. (**F**) Endogenous IP of USP7 from nuclear extracts of mESCs followed by immunoblotting of USP7, RING1B, RYBP, PCGF1, PCGF3, and PCGF5. (**G**) Endogenous IP of USP7 from nuclear extracts of mESCs with or without treatment of benzonase (250 U/ml) followed by immunoblotting of USP7, SOX2, and RING1B. (**H**) Schematic of USP7 domains and generation of truncates and point mutants. ΔTRAF, TRAF domain deficiency; ΔEnzy, catalytic region (amino acids 208 to 560) deficiency; C224A/C224S, mutations of cysteine-224 into alanine or serine. (**I**) IP of Flag from nuclear extracts of mESCs after transfection of followed by transfection with empty vector, USP7ΔTRAF, USP7ΔEnzy, C224S, or WT. (**J**) Immunoblotting of Flag and HA from HEK293T cells 5 days after transfection with HA-SOX2 and Flag-USP7WT, C224S, or C224A. (**K**) Immunoblotting of USP7 and SOX2 in shCtrl-, sh*Usp7*#2-, and sh*Usp7*#3-infected mESCs with/without treatment with cycloheximide (CHX; 10 μg/ml). Dashed lines indicate the timing for 50% drop of USP7 level after knockdown by sh*Usp7*#2 and sh*Usp7*#3, respectively. Biological replicates, $n = 3$; $^{*}P < 0.05$ and $^{***}P < 0.001$.

To further study whether USP7 stabilizes SOX2 protein by deubiquitination, we immunoprecipitated SOX2, OCT4, and NANOG proteins in mESCs infected by shCtrl or sh*Usp7*#2 and then immunoblotted Ub. Our results showed that, compared to shCtrl, sh*Usp7*#2-mediated depletion increased the ubiquitination level of SOX2 protein (Fig. 4A) but did not obviously change OCT4 and NANOG ubiquitination (Fig. 4, B and C). We then further transfected the Flag-USP7WT or Flag-USP7 (C224A/S) mutants together with HA-SOX2 and Myc-Ub plasmids into HEK293T cells and immunoprecipitated HA-SOX2 protein, followed by immunoblotting of Myc-Ub. Our results showed that overexpression of Flag-USP7WT robustly reduced the ubiquitination of HA-SOX2 generated by Myc-Ub, whereas cotransfection of Flag-USP7 (C224A/S) mutant plasmids failed to do so (Fig. 4D). Furthermore, P22077 treatment inhibited the ability of Flag-USP7WT to remove ubiquitination of HA-SOX2 (Fig. 4E). These results indicate that SOX2 is a DUB substrate of USP7. Next, we cotransfected HA-SOX2 and Myc-Ub-K48 (lysine only at the 48th amino acid site of Ub) or

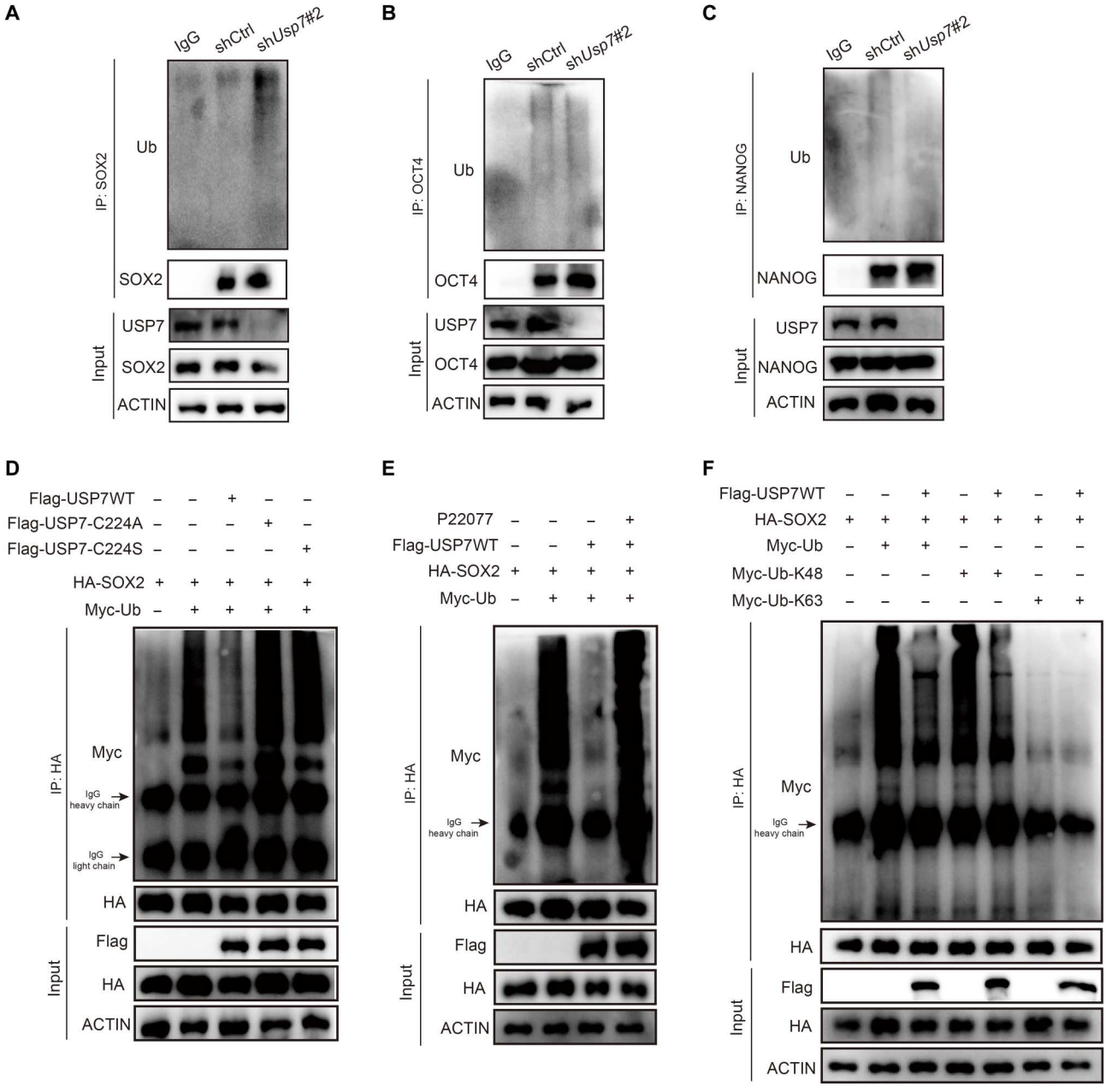

Fig. 4. USP7 deubiquitinates SOX2. (**A** to **C**) IPs of SOX2 (A), OCT4 (B), and NANOG (C) from mESCs after infection with shCtrl and sh*Usp7#2* followed by Ub immunoblotting. (**D**) IP of HA from HEK293T cells after transfection with HA-SOX2, Myc-Ub, and Flag-USP7WT or Flag-USP7C224S/A followed by immunoblotting of Myc and HA. (**E**) IP of HA from HEK293T cells after transfection with Flag-USP7WT, HA-SOX2, and Myc-Ub in the presence of P22077 (0.8 μM) treatment followed by Myc, HA, and Flag immunoblotting. (**F**) IP of HA from HEK293T cells after transfection with Flag-USP7WT, HA-SOX2, Myc-Ub, Myc-Ub-K48, or Myc-Ub-K63 followed by Myc, HA, and Flag immunoblotting. ACTIN serves as the loading control.

Myc-Ub-K63 (lysine only at the 63th amino acid site of Ub) plasmid with or without Flag-USP7WT plasmid into HEK293T cells and then immunoprecipitated HA, followed by immunoblotting of Myc. We found that cotransfection of Myc-Ub-K48 rather than Myc-Ub-K63 was able to increase the ubiquitination of HA-SOX2 protein that could be removed by Flag-USP7WT (Fig. 4F), suggesting that the Ub was added to SOX2 mainly at the 48th lysine. Together, our results demonstrated that USP7 deubiquitinates SOX2 to sustain its expression.

USP7 co-occupies lineage differentiation genes with SOX2 and/or RYBP in mESCs

We then went on to further investigate how USP7 might regulate the transcriptional network of mESCs through SOX2 and/or RYBP-vPRC1. We first examined the genome-wide occupancy of USP7 by CUT&Tag technology and compared its targets against that of SOX2 and RYBP by analyzing their published chromatin IP sequencing (ChIP-seq) datasets in mESCs (*37*, *38*). By comparing the distribution of their binding peaks, we found that a large proportion of USP7 binding peaks also exhibited either strongest or moderate SOX2 and RYBP binding signals, respectively (Fig. 5A, clusters 1 and 3), whereas strongest RYBP binding peaks were largely devoid of USP7 or SOX2 binding (Fig. 5A, cluster 2). Further, Venn diagram analysis showed that approximately 95% (7038 of 7415) of SOX2 binding genes are also co-occupied by RYBP (Fig. 5B), suggesting that SOX2 may repress gene expression through RYBP-vPRC1 complexes. USP7, SOX2, and RYBP co-occupy 4382 target genes that constitute around 44% (4382 of 9915) of USP7, 59% (4382 of 7415) of SOX2, and 22% (4382 of 19,828) of RYBP binding genes, respectively (Fig. 5B). The common targets include a group of ME genes such as *T* encoding TF Brachyury and *Hand1* known to be repressed by SOX2 (Fig. 5B) (*6*, *39*), suggesting that USP7 may repress this group of ME genes through coupling the interplay of SOX2 and RYBP-vPRC1 in mESCs. We also found that approximately 47% (4691 of 9915) of USP7 targets including PE-related genes *Gata6* and *Gata4* overlapped with RYBP bound genes only without SOX2 binding. It suggests that USP7 may repress this group of genes by RYBP-vPRC1 rather than SOX2 (Fig. 5B).

To further elaborate the ability of USP7 to repress lineage differentiation genes, we performed *Usp7* depletion or its catalytic activity inhibition by shRNA or P22077 treatment in mESCs, respectively, and analyzed gene expression. Our results showed that *Usp7* depletion increased the expression of PE, ME, and TE genes (Fig. 5C and fig. S5, A and B), whereas PE genes such as *Gata4* and *Gata6* were not derepressed by P22077 treatment (Fig. 5D and fig. S5, C and D). These results suggest that while the DUB activity of USP7 is required to repress ME and TE genes, repression of PE lineage genes may rely on its structural function rather than catalytic activity.

Since USP7 deubiquitinates SOX2 that represses ME genes, we speculate that USP7 indirectly inhibits the expression of ME genes by maintaining the level of SOX2. To test this hypothesis, we compared the differentially expressed genes between sh*Usp7*#2 versus shCtrl against USP7- and SOX2-bound genes in mESCs and found that around 16% (298 of 1811) of *Usp7* knockdown-induced dysregulated genes are co-occupied by USP7 and SOX2 (Fig. 5E), suggesting that these genes are likely directly related to USP7 and SOX2 occupancy at the chromatin. Moreover, 320 up-regulated and 182 down-regulated genes were SOX2-bound targets, respectively (fig. S5, E and F). GO analysis showed that while the 320 up-regulated genes are mainly related to embryonic organ, urinary system development, and cell fate determination (fig. S5G), the 182 down-regulated genes are largely associated with brain development (fig. S5H), being consistent with the role of SOX2 in promoting neural development (*40*).

To further verify that USP7 can inhibit the expression of ME genes through SOX2, we overexpressed control or Flag-SOX2 vector in shCtrl- and sh*Usp7*#2-infected mESCs (Fig. 5F) and found that overexpression of SOX2 rescued the expression of ME, but not PE genes (Fig. 5G). Together, our results suggest that USP7 and SOX2 together with or without RYBP co-occupy distinct lineage differentiation genes. While USP7 seems to repress ME genes through its catalytic deubiquitination of SOX2, inhibition of PE-associated genes likely lies in its noncatalytic activity.

USP7 represses ME and PE genes through its catalytic and noncatalytic functions

To further delineate the catalytic and noncatalytic functions of USP7 to regulate gene expression, we first attempted to knock out *Usp7* to obtain $Usp7^{-/-}$ mESCs for rescue experiments using CRISPR-Cas9 technology. Consistent with the sh*Usp7* knockdown results (Fig. 2C), knockout of *Usp7* in mESC pool also reduced SOX2 levels at days 4 and 7 after transfection (fig. S6A). However, we did not find that SOX2 and RING1B protein levels were down-regulated in two $Usp7^{-/-}$ clones despite that H2Bub1 levels were robustly increased as previously reported (fig. S6B) (*41*), confirming the role of USP7 in removing H2Bub1 (*42*). This discrepancy suggests that $Usp7^{-/-}$ cells replenished SOX2 and RING1B levels through compensation mechanisms to survive under the condition of USP7 deficiency and culture selection, since we noted that knockout of *Usp7* severely impaired cell viability and retarded cell growth during the process of selecting $Usp7^{-/-}$ clones likely due to the known regulation of p53 by USP7 (*30*).

To circumvent the culture adaptation and compensation problem caused by long-term deficiency of USP7, we used an auxin-inducible degradation (AID) system to rapidly deplete the exogenous Flag-$USP7^{AID}$ protein by indole-3-acetic acid (IAA) and then knocked out endogenous *Usp7* in mESCs by a pair of CRISPR-Cas9 single-guide RNAs (sgRNAs) targeting intronic sequences flanking exon 1 of *Usp7* gene (fig. S6C). We then selected *Usp7*-deficient clone 2 where the addition of IAA successfully induced rapid degradation of exogenous FLAG-$USP7^{AID}$ as shown by immunoblotting analysis (fig. S6D). We further overexpressed HA-C224S catalytic dead mutant or HA-USP7WT in clone 2 of mESCs for subsequent experiments (Fig. 6A and fig. S6, C and D). Our results showed that Flag-$USP7^{AID}$ was rapidly degraded since day 1 upon IAA addition to day 5 examined, which was accompanied with reduced SOX2 and RING1B levels (Fig. 6B). These results were consistent the shRNA-based depletion and P22077 treatment data (Fig. 2, C and I). By contrast, although RYBP and PRC2 subunits including EZH2, SUZ12, and JARID2 levels decreased at day 1, they recovered from day 3 to day 5 after IAA treatment (Fig. 6B). It suggests that USP7 unlikely directly maintains the stability of RYBP, EZH2, SUZ12, and JARID2 as it does for SOX2 and RING1B, but rather their reductions at day 1 were possibly a result of PRC1.1 and PRC2.2 complexes disassembly after diminished levels of USP7 and RING1B subunits. We found

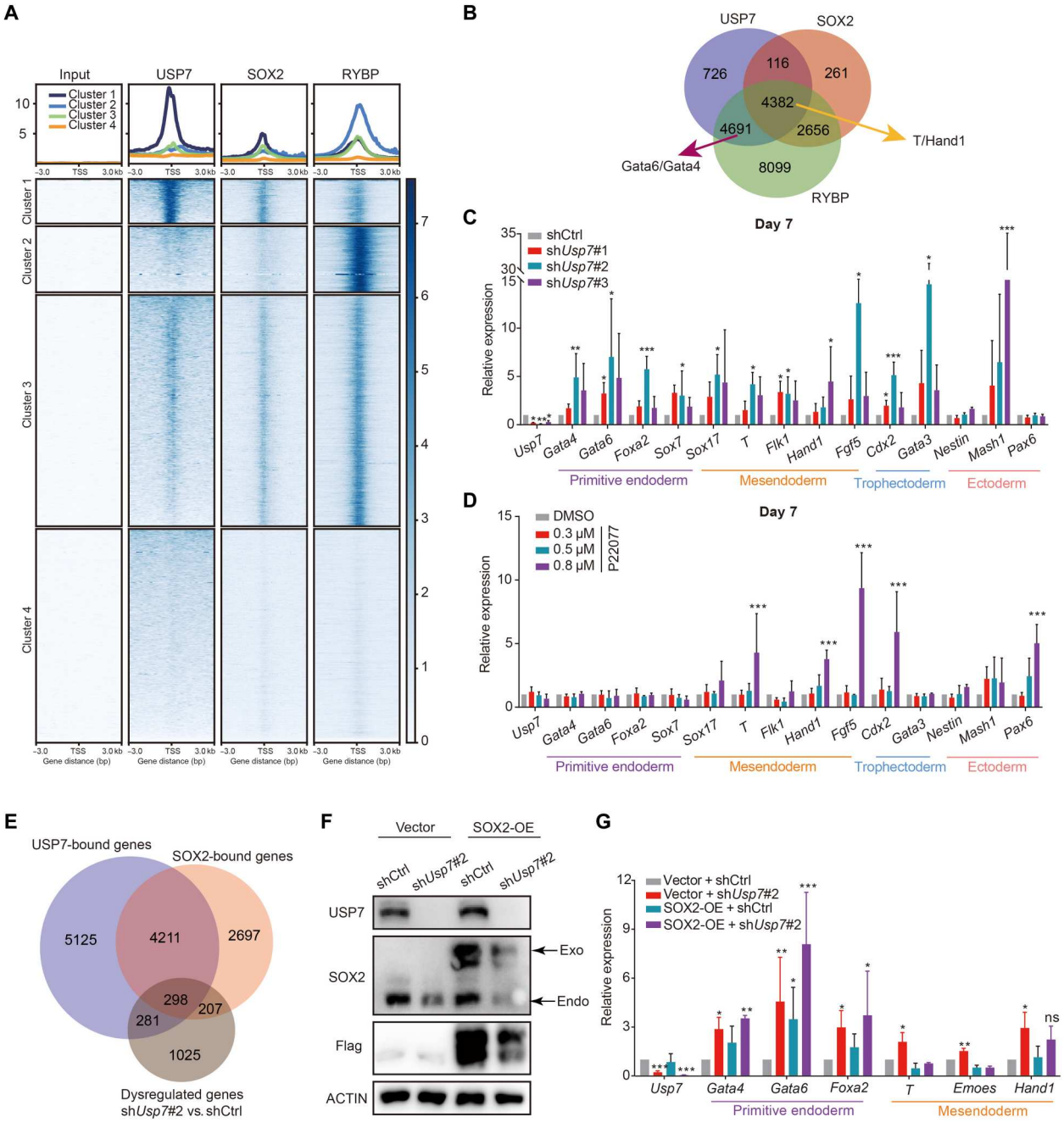

Fig. 5. USP7 co-occupies lineage differentiation genes with SOX2 and/or RYBP in mESCs. (**A**) Heatmap of USP7 CUT&Tag binding peaks distribution in correlation with the previously published SOX2 (*37*) and RYBP (*38*) ChIP-seq data in mESCs. TSS, Transcription Start Site. (**B**) Venn diagram analysis of USP7, SOX2, and RYBP binding genes in mESCs. (**C**) RT-qPCR analysis of lineage differentiation genes in mESCs 7 days after infection with shCtrl or sh*Usp7*. Means ± SD of $n = 3$ independent experiments (*$P < 0.05$, **$P < 0.01$, and ***$P < 0.001$). (**D**) RT-qPCR analysis of lineage differentiation genes in mESCs 7 days after treatment with DMSO or P22077. Means ± SD of $n = 3$ independent experiments (***$P < 0.001$). (**E**) Venn diagram analysis of differentially expressed genes in sh*Usp7*#2 versus shCtrl overlapping with SOX2- and USP7-bound genes (*37*). (**F**) Immunoblotting of USP7, SOX2, and Flag in shCtrl- or sh*Usp7*#2-infected mESCs with or without Flag-SOX2 overexpression (SOX2-OE). ACTIN serves as the loading control. (**G**) RT-qPCR analysis of genes representative of PE and ME lineages in mESCs at day 7 after infection with shCtrl or sh*Usp7*#2 together with or without Flag-SOX2 overexpression. Means ± SD of $n = 3$ independent experiments (*$P < 0.05$, **$P < 0.01$, and ***$P < 0.001$).

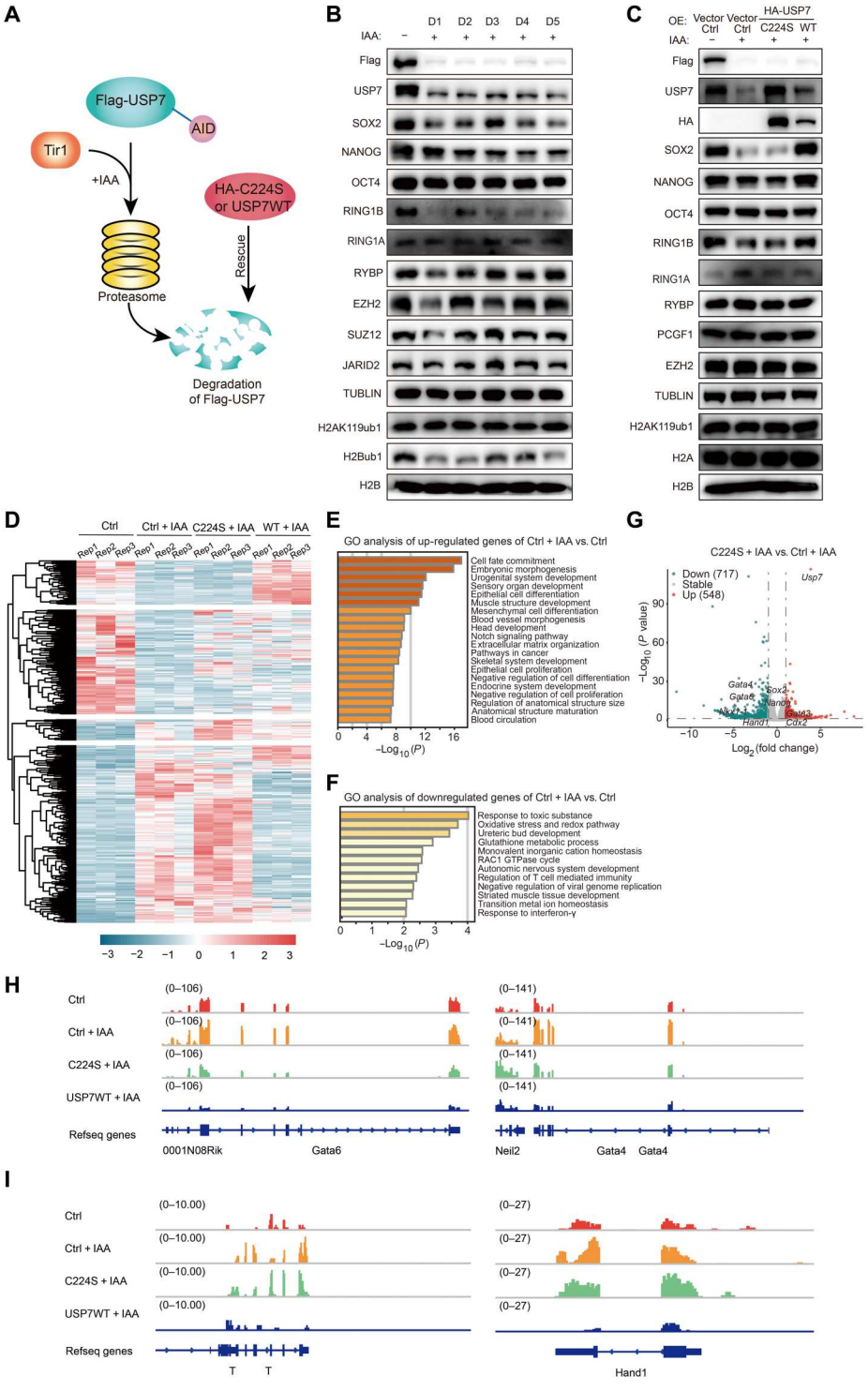

Fig. 6. USP7 represses ME and PE genes through both catalytic and noncatalytic activities. (**A**) Schematic illustrating generation of the Flag-USP7 degron system in mESCs. Addition of auxin (IAA) to cells expressing auxin-binding receptor Tir1 induces proteasomal degradation of Flag-USP7^{AID}. See also fig. S6. AID, auxin-inducible degradation. (**B**) Immunoblotting of Flag, USP7, OSN, PcG proteins, H2AK119ub1, and H2Bub1 in *Usp7*$^{-/-}$ mESCs expressing Flag-USP7^{AID} treated with IAA for the indicated time. TUBULIN and H2B serve as loading controls. (**C**) Immunoblotting of Flag, USP7, HA, OSN, PcG proteins, H2AK119ub1, and H2Bub1 in *Usp7*$^{-/-}$ mESCs expressing Flag-USP7^{AID} with overexpression of control vector, HA-USP7C224S, or HA-USP7WT treated with or without IAA for 3 days. TUBULIN and H2B serve as loading controls. (**D**) RNA-seq heatmap showing differentially expressed genes [$P < 0.05$, $\log_2$(fold change) > 1] for the cells indicated in (C). (**E** and **F**) The GO analysis of up-regulated [adjusted $P < 0.05$, $\log_2$(fold change) > 1] (E) or down-regulated [adjusted $P < 0.05$, $\log_2$(fold change) < −1] (F) gene of Ctrl + IAA versus Ctrl. GTPase, guanosine triphosphatase. (**G**) The volcano plot depicting gene expression changes between C224S + IAA versus Ctrl + IAA group. Up-regulated genes [adjusted $P < 0.05$, $\log_2$(fold change) > 1] were shown in red. Down-regulated genes [adjusted $P < 0.05$, $\log_2$(fold change) < −1] were indicated in cyan. (**H** and **I**) The Integrative Genomics Viewer (IGV) showing RNA-seq binding peaks on PE (H) and ME (I) representative genes in mESCs indicated in Fig. 6D.

that induced Flag-USP7^{AID} degradation in *Usp7* knockout background did not notably change H2AK119ub1 level despite the reduced RING1B level (Fig. 6B). This is likely attributed to the contribution of RING1A to maintaining H2AK119ub1 level (Fig. 6B), consistent with a previous study reporting that H2AK119ub1 level was reserved in mESCs with *Ring1b* deletion, while *Ring1a* was preserved (*43*). Furthermore, our results showed that overexpression of HA-C224S in contrast to HA-USP7WT failed to rescue the reduced levels of SOX2 and RING1B induced by IAA at day 3 after addition (Fig. 6C). Similar results were observed for the colony-forming efficiency of these cells (fig. S6, E and F). Therefore, these data support that the catalytic activity of USP7 is required to maintain SOX2, similar to its known deubiquitination substrate RING1B (*32*, *44*), for the self-renewal of mESCs.

To look into transcriptional changes caused by Flag-USP7^{AID} degradation together with/without HA-C224S or HA-USP7WT rescue in *Usp7*-deficient mESCs (fig. S6), we performed RNA-seq of mESCs overexpressing control vector without/with IAA addition (Ctrl/Ctrl + IAA) and HA-C224S mutant/HA-USP7WT with IAA addition (C224S + IAA/USP7WT + IAA) in triplicates. Our results showed that loss of Flag-USP7^{AID} induced by IAA addition led to differential expression of a total of 1268 genes compared to the control without IAA treatment (Ctrl + IAA versus Ctrl), among which only 291 genes were down-regulated but 977 genes were up-regulated (Fig. 6D and table S5). Consistent with shRNA-mediated *Usp7* depletion results (fig. S2, G and H), GO pathway analysis showed that most of the up-regulated genes were associated with cell fate commitment and embryonic morphogenesis (Fig. 6E). However, unlike shRNA-mediated *Usp7* knockdown (fig. S2I), the down-regulated genes were mainly involved in response to toxic substance and metabolic process (Fig. 6F), which is likely due to differential effect on gene expression caused by lentivirus-based knockdown versus IAA-induced degradation of Flag-USP7^{AID} in the endogenous *Usp7*-deficient mESCs. Nevertheless, these results support that USP7 maintains the identity of mESCs largely through repressing lineage differentiation genes. Furthermore, our results indicated that, in contrast to USP7WT (USP7WT + IAA versus Ctrl), C224S overexpression failed to rescue most of the differentially expressed genes caused by Flag-USP7^{AID} degradation (C224S + IAA versus Ctrl) (Fig. 6D), suggesting that USP7 regulates gene expression in mESCs predominantly dependent on its catalytic function. However, further comparison of gene expression between C224S + IAA and Ctrl + IAA mESCs revealed that 717 and 548 genes were down-regulated and up-regulated in C224S overexpression mESCs relative to Ctrl + IAA mESCs (Fig. 6G), respectively. We found that PE genes such as *Gata4*, *Gata6*, *Sox7*, and *Sox17* (Fig. 6H and fig. S7A), but not ME genes such as *T*, *Hand1*, *Eomes*, *Flk1*, etc. (Fig. 6I and fig. S7B), were among the down-regulated genes (C224S + IAA versus Ctrl + IAA) (Fig. 6G) that were derepressed by Flag-USP7^{AID} degradation (Ctrl + IAA versus Ctrl). It indicates that C224S overexpression was able to repress the expression of PE rather than ME genes. Together, our results suggest that USP7 represses ME and PE genes through its catalytic and noncatalytic functions, respectively.

USP7 represses PE genes through its noncatalytic structural function to maintain RYBP binding

To look into how catalytic and noncatalytic structural functions of USP7 in relation to vPRC1 and PRC2 might contribute to gene repression, we examined genome-wide occupancy of H2AK119ub1, H3K27me3, and RYBP in Ctrl, Ctrl + IAA, C224S + IAA, and USP7WT + IAA mESCs using CUT&Tag technology. Since our results showed that RYBP level decreased at day 1 but recovered at day 3 after the addition of IAA (Fig. 6, B and C), we performed CUT&Tag at day 3 to avoid the possible effect of RYBP level. Our results showed that despite the H2AK119ub1 level did not obviously change after IAA-induced Flag-USP7^{AID} degradation (Fig. 6, B and C), its enrichment signals on target genes were overall reduced in Ctrl + IAA relative to Ctrl (Fig. 7A). Overexpression of C224S in contrast to USP7WT was unable to restore H2AK119ub1 binding signals (Fig. 7A). These changes in H2AK119ub1 enrichment signals on chromatin were concomitant with the fluctuations in the levels of RING1B, the known catalytic substrate of USP7 among PRC1.1 subunits (Figs. 6C and 7A), supporting that USP7 contributes to H2AK119ub1 chromatin landscape by maintaining its major writer RING1B. Our results also showed that the changes in H3K27me3 signals were correlated with that of H2AK119ub1 (Fig. 7B), suggesting that chromatin configurations of these two histone modifications were coupled when USP7 was perturbed, both of which were largely dependent on the catalytic activity of USP7. We found that RYBP binding signals were also notably attenuated in Ctrl + IAA in comparison to Ctrl mESCs (Fig. 7C) when the level of RYBP did not change at day 3 of IAA addition (Fig. 6C), suggesting that degradation of USP7 led to disassembly of RYBP-vPRC1 on chromatin. However, we unexpectedly found that overexpression of C224S, similar to USP7WT, restored overall RYBP binding signals in C224S + IAA to the level in Ctrl mESCs (Fig. 7C). By further analyzing RYBP binding and H2AK119ub1 enrichment signals in relation to USP7 peaks, we observed that RYBP occupancy signals on USP7 bound peaks were recovered with nearly unchanged H2AK119ub1 enrichment densities by overexpression of C224S in C224S + IAA compared to Ctrl + IAA mESCs (Fig. 7D). These results suggest that USP7 deficient in catalytic activity harbored the ability to recruit RYBP on chromatin for occupying target genes even without sufficient RING1B catalyzing H2AK119ub1 (Fig. 6C).

Approximately 14% (103 of 717) of the down-regulated genes in C224S + IAA relative to Ctrl + IAA mESCs overlapped with H2AK119ub1 and RYBP target genes (Fig. 7E), suggesting that overexpression of C224S repressed these genes mainly through RYBP-PRC1 independent of its catalytic activity. Moreover, further analysis revealed that the signals of H2AK119ub1 and H3K27me3 at the promoter region of the 103 down-regulated genes (C224s + IAA versus Ctrl + IAA) were partially rescued in C224S + IAA compared to Ctrl + IAA (Fig. 7, F and G). By contrast, there was no notable difference of H2AK11ub1 and H3K27me3 signals at the promoter regions of the 4574 genes that were not down-regulated in C224S + IAA relative to Ctrl + IAA mESCs (Fig. 7, F and G) despite a similar recovery of RYBP binding signals in the transcription starting site for both groups of genes (Fig. 7H). These results suggest that the scaffold of catalytically inactive USP7 with C224S point mutation is capable of inhibiting gene expression through Polycomb system.

A closer analysis of our CUT&Tag data revealed that H2AK119ub1 and H3K27me3 signals were partially rescued at the promoter regions of down-regulated PE genes such as *Gata4* and *Gata6* accompanied with recovered RYBP binding in C224S + IAA mESCs (Fig. 7, I to K, and fig. S8, A, C, E, G, H, and J). However, while H2AK119ub1 and H3K27me3 signals also appeared to weakly recover on ME genes such as *T* and *Cdx2* (Fig. 7, L and M and fig. S8, B, D, G, and H), RYBP binding at *T* and *Cdx2* genes was not recovered in C224S + IAA (Fig. 7N and fig. S8, F and J). Together, these results suggest that while USP7 represses ME genes in a catalytic activity–dependent manner, its noncatalytic structure maintains RYBP binding on chromatin to repress PE genes via Polycomb system (Fig. 8).

DISCUSSION

Our study revealed the role of USP7 in maintaining the identity of mESCs and supports a model in which USP7 shapes the transcriptional network of mESCs not only through its catalytic activity–

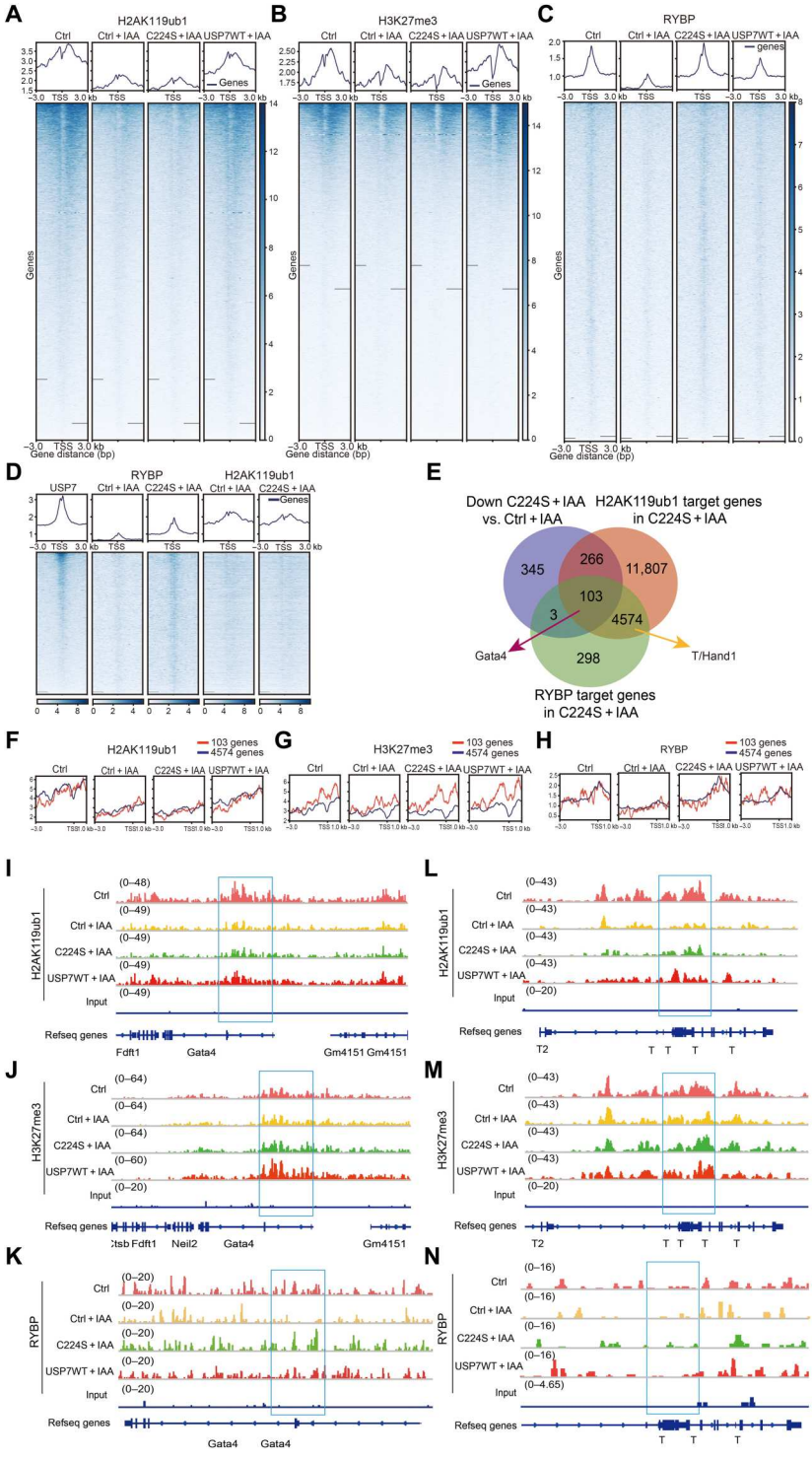

Fig. 7. USP7 represses ME genes through its noncatalytic scaffold ability to maintain RYBP binding. (**A** to **C**) Heatmaps showing H2AK119ub1, H3K27me3, and RYBP CUT&Tag signals in *Usp7*$^{-/-}$ mESCs expressing Flag-USP7^{AID} with overexpression of control vector, HA-USP7C224S, or HA-USP7WT treated with or without IAA for 3 days. (**D**) Heatmaps showing H2AK119ub1 and RYBP CUT&Tag signals in relation to wild-type mESC USP7 CUT&Tag binding peaks in *Usp7*$^{-/-}$ mESCs expressing Flag-USP7^{AID} with control vector or HA-USP7C224S overexpression after 3 days of IAA treatment. (**E**) Venn diagram analysis of the overlapping of the down-regulated genes in C224S + IAA versus Ctrl + IAA with H2AK119ub1- and RYBP-bound genes in C224S + IAA cells. (**F** to **H**) Profile plots showing the CUT&Tag signal distribution of H2AK119ub1, H3K27me3, and RYBP on the 103 and 4574 genes in *Usp7*$^{-/-}$ mESCs expressing Flag-USP7^{AID} with overexpressing of control vector, HA-USP7C224S, or HA-USP7WT and after 3 days of IAA treatment. (**I** to **N**) The IGV showing H2AK119ub1, H3K27me3, and RYBP binding signals on *Gata4* and *T* genes for cells in (A) to (C).

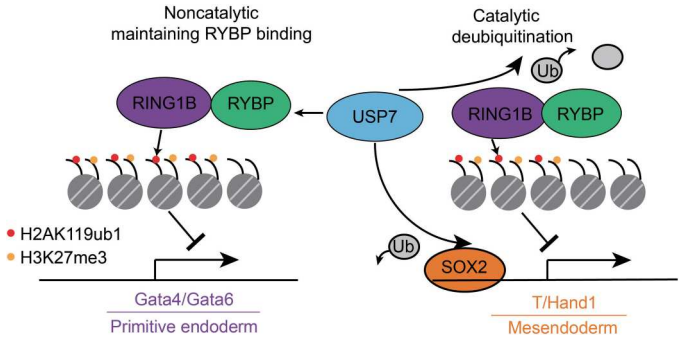

Fig. 8. The proposed model. USP7 represses ME and PE genes through catalytic ubiquitination and noncatalytic maintaining RYBP binding to chromatin, respectively.

dependent repression of ME lineage genes but also via noncatalytic structural function to repress genes associated with PE development (Fig. 8). Our results demonstrated that USP7 deubiquitinates and stabilizes SOX2 to repress genes associated with ME development. Given that OSN function as specifiers and repressors of mutually exclusive lineages (*5*, *6*, *39*), pluripotency state therefore relies on precise regulation of their levels, perturbation of which causes differentiation into different germ layers (*45*, *46*). Protein ubiquitination dynamically controlled by Ub ligases and DUBs is an important posttranslational modification that regulates protein degradation, function, and interaction (*47*). A number of DUBs have been reported to regulate pluripotency by deubiquitinating and stabilizing OSN. For example, USP3 has recently been shown to deubiquitinate and stabilize OCT4 in hESCs (*48*), whereas USP21 has been previously identified to deubiquitinate NANOG in mESCs by screening a large number of DUBs including USP7 (*19*–*21*). Nevertheless, a recent study has claimed that Bach1 regulates NANOG ubiquitination through recruitment of USP7 in hESCs (*49*). Our results support that USP7 predominantly interacts and deubiquitinates SOX2 rather than NANOG and OCT4 in mESCs (Figs. 3C and 4). These evidences collectively suggest a species-specific dependency of OSN on a major DUB for stabilization in mESCs versus hESCs. It remains to be further investigated whether USP7 may also regulate the ubiquitination of other pluripotency-associated factors such as LIN28A shown on its interacting protein list (Fig. 3A and fig. S4C).

In support of USP7 as an epigenetic regulator (*17*), our MS results showed that USP7 might interact with multiple PcG proteins including PRC2 core methyltransferase EZH1 and PRC1 subunits such as RING1B, BCOR, PCGF1, MGA, and PCGF6 (Fig. 3A and fig. S4C). Although the direct regulation of EZH1 by USP7 in mESCs needs further verification, these results are a line with the previously reported interaction of Elongin BC and PRC2-associated protein (EPOP), a PRC2 regulator (*50*), with USP7 to regulate the levels of H2Bub1, a transcription active histone modification, in mESCs (*41*). Regardless that USP7 is a known H2B DUB (*42*), our results showed reduced H2Bub1 level upon IAA-induced degradation of Flag-USP7^{AID} in *Usp7*-deficient mESCs (Fig. 6B). It suggests that other H2Bub1 Ub ligases such as RNF20/40 and DUBs such as USP22 and USP51 might be involved in regulating H2Bub1 level upon the induced degradation of exogenous Flag-USP7^{AID} in mESCs deficient in *Usp7* (*22*, *51*). At the gene transcriptional level, our RNA-seq results revealed a predominant up-regulation of genes associated with cell fate commitment induced by degradation of USP7 (Fig. 6E and table S5), which is unlikely due to the reduced H2Bub1. Therefore, it supports that USP7 largely functions as a transcriptional repressor in mESCs beyond H2Bub1. Several previous studies have demonstrated that USP7 exists in PRC1.1 as a DUB regulator (*11*, *15*). In line with these studies, our IP results confirmed the interaction of USP7 with RING1B, RYBP, PCGF1, and PCGF3/5 although its association with MGA and PCGF6 remains to be verified (Fig. 3F). In line with our results, very recent studies have identified MGA and PCGF6 as the new substrates of USP7 (*52*, *53*). Thus, these together with our results suggest that USP7 may assemble into multiple RYBP-vPRC1 complexes than previously thought. Consistent with the previous study showing that USP7 interacts and deubiquitinates RING1B to stabilize PRC1 (*32*), our results also showed that USP7 depletion reduced RING1B level in a catalytic activity–dependent manner (Fig. 6, B and C). This is likely responsible for the observed attenuation of H2AK119ub1 enrichment signals concomitant with depression of lineage differentiation genes upon IAA-induced degradation of USP7 that was not rescued by C224S mutant (Fig. 7A). The changes in H3K27me3 enrichment signal are similar, but not as robust as H2AK119ub1 (Fig. 7B). These results collectively support that catalytic activity of RING1B in vPRC1 is essential to Polycomb-mediated gene repression in mESCs through H2AK119ub1 deposition as previously reported (*13*, *14*). Our results showed that USP7 contributes to Polycomb chromatin–mediated repression of ME lineage genes in a catalytic activity–dependent manner. This is consistent with the previously reported role of BCOR-PRC1.1 in repressing key developmental regulators in hESCs (*15*).

In contrast, our results demonstrated that rapid IAA-induced degradation of USP7 triggered a decreased RYBP level at day 1, which then recovered at day 3 and onward (Fig. 6B). Therefore, it is unlikely that USP7 directly deubiquitinates and stabilizes RYBP similar to RING1B. Although RYBP level was recovered at day 3 (Fig. 6B), its genome-wide binding signals were obviously reduced at day 3 after IAA-induced degradation of USP7 (Fig. 7C). It suggests that USP7 depletion induced disassembly of PRC1 and dissociation of RYBP from chromatin. Nevertheless, USP7 deficient in its deubiquitination function is able to restore RYBP binding on chromatin for repressing PE-associated genes, suggesting that repression of PE genes is dependent on recruitment of RYBP to chromatin by noncatalytic structural function of USP7. These results are consistent with the previous studies reporting that RYBP may regulate PRC1 stability and maintain H2AK119ub1 at vPRC1 targets (*54*, *55*).

In this study, we report that USP7 deubiquitinates and stabilizes SOX2 to repress genes associated with ME development in mESCs. One limitation of our study is that it is unclear if USP7 plays a role in establishing pluripotency during early mouse embryonic development in part by stabilizing SOX2 despite the observed positive correlation between *Usp7* and *Sox2* expression in ICM. *Usp7* knockout in mice causes early embryonic lethality, and blastocyst of *Usp7* deficiency fails to proliferate presumably because of its catalytic regulation of MDM2-p53 pathway (*56*). ICM cells in blastocyst of *Usp7* deficiency mouse embryo were also reported to differentiate extensively, and *p53* knockout partially rescued the phenotype of *Usp7* knockout mice (*56*). It suggests that *Usp7* knockout mice phenotype is unlikely exclusively dependent on its regulation of p53. Whether

its catalytic activity–dependent stabilization of SOX2 and/or structural function to repress genes associated with PE development through RYBP-vPRC1 observed in mESCs model contribute to early mouse embryonic development needs further investigation. Moreover, USP7 plays a very important role in tumorigenesis through its enzymatic regulation of MDM2-p53 pathway and many other proteins, various inhibitors to block its catalytic activities have been developed in the past for potential cancer treatment. Its noncatalytic structural function awaits further study in the context of tumorigenic process that will likely provide important insights into development of therapeutic interventions by targeting USP7.

In summary, our study unravels the molecular mechanism by which USP7 shape the pluripotent transcriptional network to maintain mESC identity through both catalytic and noncatalytic structural activity–dependent repressions of lineage differentiation genes. Therefore, our study reveals a novel role of USP7 in regulating gene transcription that has broad implications with understanding its function in diverse biological processes.

MATERIALS AND METHODS

Animal statement

All in vivo experiments were performed in accordance with protocols from the Institutional Animal Care. The experimental protocol and ethics were approved by the Animal Care Facility of Zhejiang University (ZJU20220013). Day 3.5 embryos were collected from C57BL6 mice (8 weeks old) for immunofluorescent staining experiments. For teratoma formation experiments, BALB/cJGpt-*Foxn1*^{nu}/Gpt (nude) (male, 4 to 5 weeks old) were purchased from GemPharmatech (Nanjing, China) and bred in the Experimental Animal Facility of Zhejiang University.

Cell culture

Mouse E14 embryonic stem cells [CRL-1821, American Type Culture Collection (ATCC)] were cultured on 0.1% gelatin (40108ES60, Yeasen, China)–coated plates in Dulbecco's modified Eagel's medium (DMEM) with glucose (4.5 g/liter; 10-013-CVR, Corning), supplemented with 15% fetal bovine serum (FBS; catalog no. 10099, Gibco), GlutaMAX (35050-61, Gibco), minimum essential medium nonessential amino acids (11140-050, Gibco), penicillin/streptomycin (Gibco), 0.1 mM β-mercaptoethanol (M3148, Sigma-Aldrich), and LIF (1000 U/ml; ESG1107, Millipore). Naïve mESCs were cultured in N2/B27 2i/LIF media comprising 1:1 mix of DMEM/F12 and Neurobasal medium containing N2 and B27 supplements, penicillin/streptomycin, 0.1 mM β-mercaptoethanol, 2 mM L-glutamine, and LIF supplemented with 1 μM PD03259010 and 3 μM CHIR99021 (STEMCELL Technologies) on irradiated CF1 MEF (0304-500, Innovative Cellular Therapeutics Co. Ltd.) feeder layer. HEK293T cells (CRL-11268, ATCC), HFFs (SCRC-1041, ATCC), and MEFs were cultured in DMEM with glucose (4.5 g/liter), supplemented with 10% FBS. hiPSCs and H9 hESC line (WA09, WiCell) were cultured on Matrigel (BD Biosciences)–coated plate in complete mTeSR1 medium (STEMCELL Technologies) as previously described (*57*).

Gene knockdown, knockout, and overexpression in mESCs

For target gene knockdown, sequences of three shRNAs against *Usp7* (table S1) and scramble sequences were inserted into a pLKO lentiviral vector (Addgene). Lentiviruses were produced by cotransfection of pLKO-shRNA, psPAX2, and pMD2.G into HEK293T cells. At 24, 48, and 72 hours after transfection, viral supernatant were harvested. For gene knockout, mESCs were transfected with a px330-Cas9 plasmid (Addgene) together with a pair of sgRNAs targeting intronic sequences flanking exon1 of *Usp7* gene using Lipofectamine 2000 (Life Technologies). After transfection, cells were cultured under puromycin (2 μg/ml) for 3 days. Cells were collected for immunoblotting analysis at days 0, 4, and 7 after transfection, and single clones were also picked for subsequent experiments. To overexpress target genes, the coding sequences were cloned into pB-CAG vectors and then cotransfected with pBASE plasmid into mESCs using Lipofectamine 2000. After transfection, the cells were cultured under puromycin (2 μg/ml) or hygromycin (200 μg/ml), respectively.

Teratoma formation and histological analysis

A total of 1×10^6 mESCs 7 days after infection with shCtrl or sh*Usp7*#2 were suspended in 100 μl of DMEM with 30% Matrigel (354277, BD Biosciences) and subcutaneously injected into the groin of the nude mice for teratoma formation. Teratomas were harvested from the mice 5 weeks after injection, and their sizes from different groups were measured and quantified. Histological analysis was performed by the Histology Core Facility at School of Medicine of Zhejiang University.

Construction of *Usp7* knockout mESCs line with auxin-inducible degron of Flag-USP7

To construct the *Usp7*-deficient mESCs line with AID of exogenous Flag-USP7 (Flag-USP7^{AID}) (*58*), we first cloned mouse *Usp7* coding sequence into a pB-CAG-3 × Flag-AID vector (hygromycin-resistant) and cotransfected with the E3 ligase expression plasmid for the AID system (PB-Tir1; neomycin-resistant) and a pBASE plasmid expressing the transposase into mESCs. Those vectors were provided by Y. Yin's laboratory at Zhejiang University School of Medicine. After selection with antibiotics (G418, 280 μg/ml; hygromycin, 200 μg/ml) for 7 days, endogenous *Usp7* gene was deleted by the CRISPR-Cas9 approach using a pair of sgRNAs targeting intronic sequences flanking exon1, and single clones were then picked. Clones with homozygous deletion of endogenous *Usp7* and rapid degradation of exogenous Flag-USP7^{AID} upon addition of the auxin analog IAA (500 μM) were used for downstream experiments. The pB-CAG-3 × HA-C224S (USP7 catalytically dead mutation) and pB-CAG-3 × HA-USP7WT (USP7 wild-type) were overexpressed in Flag-USP7^{AID} cell line for rescue experiments.

RNA extraction, reverse transcription qPCR, and RNA-seq

Total RNA was extracted with RNAiso Plus (9109, Takara) following the manufacturer's instructions. cDNA was then produced by reverse transcription (RT) using ReverTra Ace qPCR RT Master Mix (FSQ-201, TOYOBO). RT-qPCR was performed via SYBR Premix Ex Taq (RR420A, Takara) and the Roche Light Cycler 480. The expression was normalized to the β-*Actin*. All the primers used are listed in table S1. RNA-seq library preparation and sequencing were performed by Novogene in Tianjin, China on NovaSeq 6000 with 150 base pairs (bp) per read length and paired end.

ChIP-seq and ChIP-qPCR

ChIP-seq was performed as previously described (*57*). ChIP-qPCR was performed via SYBR Premix Ex Taq (RR420A, Takara) and the Roche Light Cycler 480. *Gapdh* served as a control. ChIP-qPCR primers were listed in the table S1.

Alkaline phosphatase staining

A total of 2×10^3 mESCs were seeded in a six-well plate for 7 days. The alkaline phosphatase assay was performed with the BCIP/NBT Alkaline Phosphatase Color Development Kit (C3206, Beyotime Biotechnology) according to the manufacturer′s instructions.

Flow cytometry

For cell cycle analysis, 2×10^5 to 1×10^6 mESCs 6 days after infection with shCtrl, sh*Usp7*#2 or sh*Usp7*#3 lentiviruses were collected and fixed in chilled 75% ethanol and stored at −20°C overnight. DNA staining was performed with a cell cycle staining kit (40301ES50, Yeasen) according to the manufacturer′s instructions. For apoptosis analysis of mESCs after *Usp7* knockdown, the cells were infected with shCtrl, sh*Usp7*#2, or sh*Usp7*#3 lentiviruses and then selected in the culture medium supplemented with puromycin (2 μg/ml) for 3 days. For apoptosis analysis of mESCs after P22077 treatment, the cells were treated with dimethyl sulfoxide (DMSO), 0.3, 0.5, and 0.8 μM P22077 for 6 days. Then, the cells after infection or treatment were harvested by incubation in 0.05% trypsin-EDTA (Gibco) and washed once with phosphate-buffered saline (PBS). Annexin V staining was performed according to the protocol of annexin V–fluorescein isothiocyanate/propidium iodide apoptosis detection kit (A211-01, Vazyme). Flow cytometric data were collected on a flow cytometer (BD Cytomic FC 500MCL) and analyzed by the FlowJo software (v7.6).

Immunofluorescence

Immunofluorescent staining was performed according to standard procedures. The required antibody information is presented in table S2. Immunofluorescence was observed using Olympus FV3000 confocal microscope.

Ubiquitination assay

Myc-Ub, Myc-Ub-K48, or Myc-Ub-K63 plasmids were provided by D. Wang′s laboratory at Zhejiang University School of Medicine for ubiquitination assay. HA-SOX2 sequences were cloned into a pcDNA5 vector. Plasmids were transfected into HEK293T cells via polyethylenimine. For the assay of ubiquitination, cells were resuspended in IP buffer [50 mM tris (pH 7.8), 150 mM NaCl, 1% (v/v) NP-40, and 10% (v/v) glycerol] + 2% SDS, heated at 100°C for 10 min, and then diluted by 10-time dilution of IP buffer for 1-hour lysis. Proteins were immunoprecipitated from cell lysates with indicated antibodies, and then the ubiquitination of indicated proteins was detected by Western blot analysis.

Co-IP and Western blot

Cells were lysed in IP buffer. For extraction of nuclear proteins, the cells were lysed by nucleocytoplasmic separation kit (P0027, Beyotime Biotechnology, China) according to the manufacturer′s instructions. For IP, cell lysates were incubated with the indicated antibodies at 4°C overnight, and protein A/G plus magnetic beads were added and incubated for another 4 hours. After washing five times with PBS, protein SDS loading buffer was added and boiled for 5 min. Western blotting was performed according to standard procedures.

Mass spectrometry

IP samples were prepared, proteins were separated by one-dimensional gel electrophoresis, and peptides were prepared as previously described (*59*). Briefly, for data-dependent acquisition (DDA) identification, each lane was cut into five parts. For data-independent acquisition (DIA) quantification, the five parts were further combined into two parts, with one part containing the target proteins and the other with IgG heavy/light chains. Each gel band was cut into 2-mm^3 pieces, followed by reduction with 10 mM tris(2-carboxyethyl)phosphine hydrochloride in 25 mM NH_4HCO_3 at 25°C for 1 hour, alkylation with 55 mM IAA in 25 mM NH_4HCO_3 solution at 25°C in the dark for 30 min, and sequential tryptic digestion at an enzyme concentration of 10 ng/μl at 37°C for overnight. Tryptic-digested peptides were extracted using 50% acetonitrile (ACN)/5% formic acid (FA) for the first time and 75% ACN/0.1% FA for the second time. After that, peptide solutions were dried under vacuum and further purified by Pierce C18 Spin Tips (Thermo Fisher Scientific).

For DDA MS data acquisition, a total of 15 DDA raw data files from three protein-complex samples (five fractions for each sample) were generated. Peptides were separated by Ultimate 3000 nanoLC-MS/MS system (Dionex LC Packings) equipped with a 15 cm–by–75 μm inside diameter (ID) fused silica column packed with 1.9-μm 100-Å C18 (National Institute of Biological Sciences, Beijing, China). After injection, peptides were trapped at 6 μl/min on a 20 mm–by–75 μm ID trap column (Thermo Fisher Scientific, Waltham, MA) packed with 3-μm 100-Å C18 aqua in 0.1% FA. Peptides were separated along a 60-min 7 to 30% linear LC gradient (buffer A, 2% ACN and 0.1% FA; buffer B, 98% ACN and 0.1% FA) at the flow rate of 300 nl/min. Eluted peptides were ionized at a potential of +2.1 kV into a Orbitrap Exploris 480 equipped with FAIMS Pro (Thermo Fisher Scientific, Waltham, MA). Intact masses were measured at resolution 60,000 [at a mass/charge ratio (m/z) of 200] in the Orbitrap using normalized AGC target value of 300% and cycle time setting of 1 s. The peptide signals (charge states 2 to 6) were submitted to MS/MS in the HCD cell (1.6–atomic mass unit isolation width and 30% normalized collision energy). MS/MS spectra were acquired at a resolution of 15,000 (at an m/z of 200) in the Orbitrap using normalized AGC target value of 75%, a maximum IT of 22 ms. Dynamic exclusion was applied with a repeat count of 1 and an exclusion time of 50s.

DIA MS data acquisition

For each DIA MS run, 400 ng of peptides were injected. The LC configuration for DIA data acquisition is as the same as for DDA data acquisition. The DIA MS setting was described in detail as follows. A full MS scan was acquired by analyzing 390 to 1010 m/z at a resolution of 60,000 (at an m/z of 200) in the Orbitrap using normalized AGC target value of 300% and maximum IT of 50 ms. Then, the MS/MS scans were acquired, each with a resolution of 30,000 at an m/z of 200, normalized AGC target value of 2000%, and normalized collision energy as 32%, with the default charge state set to 3 and a maximum IT set to 54 ms. For the FAIMS CV of −68 V, the MS scan range is 400 to 585 m/z, the isolation window is 15 m/z, and the window overlap is 1 m/z, and the number of Windows is 12. For the FAIMS CV of −48 V, the MS scan range is 585 to 1000 m/z, the isolation window is 20 m/z, the window

overlap is 1 *m*/*z*, and the number of Windows is 20. The PPI of MS data was performed by STRING database (*60*).

Glycerol gradient assay

The glycerol gradient was prepared using 10 and 40% glycerol solutions (IP buffer, 1× protease inhibitor in nuclease-free water) in 15 ml of Beckman tube and kept at 4°C. Cells were lysed in 500 ml of IP buffer with 1× protease inhibitor and spun down at 12,000*g* for 10 min at 4°C to remove the debris. Clear lysates were added on the top of a 10 to 40% of glycerol gradient and then centrifuged at 32,000 rpm with a SW40Ti rotor for 18 hours. The resulting gradient was then fractionated every 320 ml. Thirty-seven fractions were collected and subjected to Western blot.

CUT&Tag

We used the Hyperactive In-Situ ChIP Library Prep Kit for Illumina (pG-Tn5) (TD901, Vazyme, China) to construct CUT&Tag libraries according to the manufacturer's instructions. Then, the CUT&Tag libraries were sent to Novogene (Tianjin, China) for sequencing on NovaSeq 6000 with 150 bp per read length and paired end.

Microarray, single-cell RNA-seq, and bulk RNA-seq analysis

Microarray gene expression data of mESCs and MEFs (GSE71255) were analyzed with GEO2R with a fold change of >2.0 and adjusted $P < 0.05$. Single-cell RNA-seq gene expression processed data during early mouse embryonic development (GSE84892) was analyzed using R. The correlation between *Usp7* and lineage marker genes was analyzed by Corrplot (v0.92). For bulk RNA-seq analysis, the FASTQ data were trimmed with fastp (*61*) and then mapped to mouse genome assembly mm10 via HISAT2 (*62*) to generate count files. Differentially expressed genes were generated by DESeq2 (*63*) with a fold change of >2.0 and $P < 0.05$. The heatmaps were generated by R package heatmap (version 1.0.12), and gene annotations were performed using R package (clusterProfiler) (v4.2.2). GO analysis was performed on www.metascape.org.

ChIP-seq analysis

The FASTQ data were trimmed with fastp and mapped to mouse genome assembly mm10 via Bowtie2 in paired-end mode (*64*). Peaks were called by MACS2 (*65*). ChIP-seq enriched regions were visualized with the Integrative Genomics Viewer (IGV) (*66*). Heatmaps and profile plots were generated by deepTools2 (3.3.2) (*67*).

CUT&Tag analysis

The CUT&Tag data processing and analysis were referred to https://yezhengstat.github.io/CUTTag_tutorial/ (version 10 August 2020, accessed date: 9 July 2021). Briefly, the fastq files were checked by FastQC for quality control, and then aligned to mm10 and *Escherichia coli* genome (for spike-in calibration) by Bowtie2 using parameters: --end-to-end --very-sensitive --no-mixed --no-discordant --phred33 -I 10 -X 700 (*64*). The duplication of Input was removed by Picard (https://broadinstitute.github.io/picard/, version 2.25.0, accessed date: 9 July 2021). Mapped reads were filtered and file format conversion were performed by samtools. Read pairs that are on the same chromosome and fragment length less than 1000 bp were kept. Spike-in calibration was performed by Bedtools (*68*). Peak calling was performed by SEACR (*69*). Heatmaps and profiles plots were generated by deepTools2 (*67*) (3.3.2). CUT&Tag enriched regions were visualized with the IGV (*66*).

Supplementary Materials

This PDF file includes:
Figs. S1 to S8
Legends for tables S1 to S5

Other Supplementary Material for this manuscript includes the following:
Tables S1 to S5

View/request a protocol for this paper from *Bio-protocol*.

REFERENCES AND NOTES

1. S. H. Orkin, J. Wang, J. Kim, J. Chu, S. Rao, T. W. Theunissen, X. Shen, D. N. Levasseur, The transcriptional network controlling pluripotency in ES cells. *Cold Spring Harb. Symp. Quant. Biol.* **73**, 195–202 (2008).
2. M. Li, J. C. I. Belmonte, Ground rules of the pluripotency gene regulatory network. *Nat. Rev. Genet.* **18**, 180–191 (2017).
3. L. A. Boyer, T. I. Lee, M. F. Cole, S. E. Johnstone, S. S. Levine, J. P. Zucker, M. G. Guenther, R. M. Kumar, H. L. Murray, R. G. Jenner, D. K. Gifford, D. A. Melton, R. Jaenisch, R. A. Young, Core transcriptional regulatory circuitry in human embryonic stem cells. *Cell* **122**, 947–956 (2005).
4. R. A. Young, Control of the embryonic stem cell state. *Cell* **144**, 940–954 (2011).
5. K. M. Loh, B. Lim, A precarious balance: Pluripotency factors as lineage specifiers. *Cell Stem Cell* **8**, 363–369 (2011).
6. J. Shu, C. Wu, Y. Wu, Z. Li, S. Shao, W. Zhao, X. Tang, H. Yang, L. Shen, X. Zuo, W. Yang, Y. Shi, X. Chi, H. Zhang, G. Gao, Y. Shu, K. Yuan, W. He, C. Tang, Y. Zhao, H. Deng, Induction of pluripotency in mouse somatic cells with lineage specifiers. *Cell* **153**, 963–975 (2013).
7. L. Morey, A. Santanach, L. Di Croce, Pluripotency and epigenetic factors in mouse embryonic stem cell fate regulation. *Mol. Cell. Biol.* **35**, 2716–2728 (2015).
8. L. Di Croce, K. Helin, Transcriptional regulation by Polycomb group proteins. *Nat. Struct. Mol. Biol.* **20**, 1147–1155 (2013).
9. A. Piunti, A. Shilatifard, The roles of Polycomb repressive complexes in mammalian development and cancer. *Nat. Rev. Mol. Cell Biol.* **22**, 326–345 (2021).
10. R. Cao, L. Wang, H. Wang, L. Xia, H. Erdjument-Bromage, P. Tempst, R. S. Jones, Y. Zhang, Role of histone H3 lysine 27 methylation in Polycomb-group silencing. *Science* **298**, 1039–1043 (2002).
11. Z. Gao, J. Zhang, R. Bonasio, F. Strino, A. Sawai, F. Parisi, Y. Kluger, D. Reinberg, PCGF homologs, CBX proteins, and RYBP define functionally distinct PRC1 family complexes. *Mol. Cell* **45**, 344–356 (2012).
12. N. P. Blackledge, R. J. Klose, The molecular principles of gene regulation by Polycomb repressive complexes. *Nat. Rev. Mol. Cell Biol.* **22**, 815–833 (2021).
13. N. P. Blackledge, N. A. Fursova, J. R. Kelley, M. K. Huseyin, A. Feldmann, R. J. Klose, PRC1 catalytic activity is central to Polycomb system function. *Mol. Cell* **77**, 857–874 e9 (2020).
14. S. Tamburri, E. Lavarone, D. Fernandez-Perez, E. Conway, M. Zanotti, D. Manganaro, D. Pasini, Histone H2AK119 mono-ubiquitination is essential for polycomb-mediated transcriptional repression. *Mol. Cell* **77**, 840–856.e5 (2020).
15. Z. Wang, M. D. Gearhart, Y.-W. Lee, I. Kumar, B. Ramazanov, Y. Zhang, C. Hernandez, A. Y. Lu, N. Neuenkirchen, J. Deng, J. Jin, Y. Kluger, T. A. Neubert, V. J. Bardwell, N. B. Ivanova, A non-canonical BCOR-PRC1.1 complex represses differentiation programs in human ESCs. *Cell Stem Cell* **22**, 235–251.e9 (2018).
16. N. A. Fursova, N. P. Blackledge, M. Nakayama, S. Ito, Y. Koseki, A. M. Farcas, H. W. King, H. Koseki, R. J. Klose, Synergy between variant PRC1 complexes defines Polycomb-mediated gene repression. *Mol. Cell* **74**, 1020–1036.e8 (2019).
17. R. Rawat, D. T. Starczynowski, P. Ntziachristos, Nuclear deubiquitination in the spotlight: The multifaceted nature of USP7 biology in disease. *Curr. Opin. Cell Biol.* **58**, 85–94 (2019).
18. I.-I. Kuan, K.-H. Liang, Y.-P. Wang, T.-W. Kuo, Y.-J. J. Meir, S. C.-Y. Wu, S.-C. Yang, J. Lu, H.-C. Wu, EpEX/EpCAM and Oct4 or Klf4 alone are sufficient to generate induced pluripotent stem cells through STAT3 and HIF2α. *Sci. Rep.* **7**, 41852 (2017).
19. J. Jin, J. Liu, C. Chen, Z. Liu, C. Jiang, H. Chu, W. Pan, X. Wang, L. Zhang, B. Li, C. Jiang, X. Ge, X. Xie, P. Wang, The deubiquitinase USP21 maintains the stemness of mouse embryonic stem cells via stabilization of Nanog. *Nat. Commun.* **7**, 13594 (2016).

20. S.-K. Kwon, D.-H. Lee, S.-Y. Kim, J.-H. Park, J. Choi, K.-H. Baek, Ubiquitin-specific protease 21 regulating the K48-linked polyubiquitination of NANOG. *Biochem. Biophys. Res. Commun.* **482**, 1443–1448 (2017).
21. X. Liu, Y. Yao, H. Ding, C. Han, Y. Chen, Y. Zhang, C. Wang, X. Zhang, Y. Zhang, Y. Zhai, P. Wang, W. Wei, J. Zhang, L. Zhang, USP21 deubiquitylates Nanog to regulate protein stability and stem cell pluripotency. *Signal Transduct. Target. Ther.* **2**, 16024 (2016).
22. G. Fuchs, E. Shema, R. Vesterman, E. Kotler, Z. Wolchinsky, S. Wilder, L. Golomb, A. Pribluda, F. Zhang, M. Haj-Yahya, E. Feldmesser, A. Brik, X. Yu, J. Hanna, D. Aberdam, E. Domany, M. Oren, RNF20 and USP44 regulate stem cell differentiation by modulating H2B monoubiquitylation. *Mol. Cell* **46**, 662–673 (2012).
23. L. Morey, L. Aloia, L. Cozzuto, S. A. Benitah, L. Di Croce, RYBP and Cbx7 define specific biological functions of polycomb complexes in mouse embryonic stem cells. *Cell Rep.* **3**, 60–69 (2013).
24. A. M. Farcas, N. P. Blackledge, I. Sudbery, H. K. Long, J. F. McGouran, N. R. Rose, S. Lee, D. Sims, A. Cerase, T. W. Sheahan, H. Koseki, N. Brockdorff, C. P. Ponting, B. M. Kessler, R. J. Klose, KDM2B links the Polycomb repressive complex 1 (PRC1) to recognition of CpG islands. *eLife* **1**, e00205 (2012).
25. J. He, L. Shen, M. Wan, O. Taranova, H. Wu, Y. Zhang, Kdm2b maintains murine embryonic stem cell status by recruiting PRC1 complex to CpG islands of developmental genes. *Nat. Cell Biol.* **15**, 373–384 (2013).
26. X. Wu, J. V. Johansen, K. Helin, Fbxl10/Kdm2b recruits polycomb repressive complex 1 to CpG islands and regulates H2A ubiquitylation. *Mol. Cell* **49**, 1134–1146 (2013).
27. E. Posfai, S. Petropoulos, F. R. O. de Barros, J. P. Schell, I. Jurisica, R. Sandberg, F. Lanner, J. Rossant, Position- and Hippo signaling-dependent plasticity during lineage segregation in the early mouse embryo. *eLife* **6**, e22906 (2017).
28. J. Wray, T. Kalkan, A. G. Smith, The ground state of pluripotency. *Biochem. Soc. Trans.* **38**, 1027–1032 (2010).
29. D. Huo, Z. Yu, R. Li, M. Gong, S. Sidoli, X. Lu, Y. Hou, Z. Dai, Y. Kong, G. Liu, O. N. Jensen, W. Xie, K. Helin, C. Xiong, G. Li, Y. Zhang, X. Wu, CpG island reconfiguration for the establishment and synchronization of polycomb functions upon exit from naive pluripotency. *Mol. Cell* **82**, 1169–1185.e7 (2022).
30. S.-M. Qi, G. Cheng, X.-D. Cheng, Z. Xu, B. Xu, W.-D. Zhang, J.-J. Qin, Targeting USP7-mediated deubiquitination of MDM2/MDMX-p53 pathway for cancer therapy: Are we there yet? *Front. Cell Dev. Biol.* **8**, 233 (2020).
31. E. Lecona, S. Rodriguez-Acebes, J. Specks, A. J. Lopez-Contreras, I. Ruppen, M. Murga, J. Munoz, J. Mendez, O. Fernandez-Capetillo, USP7 is a SUMO deubiquitinase essential for DNA replication. *Nat. Struct. Mol. Biol.* **23**, 270–277 (2016).
32. P. de Bie, D. Zaaroor-Regev, A. Ciechanover, Regulation of the Polycomb protein RING1B ubiquitination by USP7. *Biochem. Biophys. Res. Commun.* **400**, 389–395 (2010).
33. M. Altun, H. B. Kramer, L. I. Willems, J. L. McDermott, C. A. Leach, S. J. Goldenberg, K. G. Kumar, R. Konietzny, R. Fischer, E. Kogan, M. M. Mackeen, J. McGouran, S. V. Khoronenkova, J. L. Parsons, G. L. Dianov, B. Nicholson, B. M. Kessler, Activity-based chemical proteomics accelerates inhibitor development for deubiquitylating enzymes. *Chem. Biol.* **18**, 1401–1412 (2011).
34. D. J. Rodda, J.-L. Chew, L.-H. Lim, Y.-H. Loh, B. Wang, H.-H. Ng, P. Robson, Transcriptional regulation of nanog by OCT4 and SOX2. *J. Biol. Chem.* **280**, 24731–24737 (2005).
35. S. Bhattacharya, D. Chakraborty, M. Basu, M. K. Ghosh, Emerging insights into HAUSP (USP7) in physiology, cancer and other diseases. *Signal Transduct. Target. Ther.* **3**, 17 (2018).
36. M. Hu, P. Li, M. Li, W. Li, T. Yao, J. W. Wu, W. Gu, R. E. Cohen, Y. Shi, Crystal structure of a UBP-family deubiquitinating enzyme in isolation and in complex with ubiquitin aldehyde. *Cell* **111**, 1041–1054 (2002).
37. C. Galonska, M. J. Ziller, R. Karnik, A. Meissner, Ground state conditions induce rapid reorganization of core pluripotency factor binding before global epigenetic reprogramming. *Cell Stem Cell* **17**, 462–470 (2015).
38. J. A. Zepeda-Martinez, C. Pribitzer, J. Wang, D. Bsteh, S. Golumbeanu, Q. Zhao, T. R. Burkard, B. Reichholf, S. K. Rhie, J. Jude, H. F. Moussa, J. Zuber, O. Bell, Parallel PRC2/cPRC1 and vPRC1 pathways silence lineage-specific genes and maintain self-renewal in mouse embryonic stem cells. *Sci. Adv.* **6**, eaax5692 (2020).
39. N. Montserrat, E. Nivet, I. Sancho-Martinez, T. Hishida, S. Kumar, L. Miquel, C. Cortina, Y. Hishida, Y. Xia, C. R. Esteban, J. C. Izpisua Belmonte, Reprogramming of human fibroblasts to pluripotency with lineage specifiers. *Cell Stem Cell* **13**, 341–350 (2013).
40. S. Zhang, W. Cui, Sox2, a key factor in the regulation of pluripotency and neural differentiation. *World J. Stem Cells* **6**, 305–311 (2014).
41. R. Liefke, V. Karwacki-Neisius, Y. Shi, EPOP interacts with elongin BC and USP7 to modulate the chromatin landscape. *Mol. Cell* **64**, 659–672 (2016).
42. A. J. Cole, R. Clifton-Bligh, D. J. Marsh, Histone H2B monoubiquitination: Roles to play in human malignancy. *Endocr. Relat. Cancer* **22**, T19–T33 (2015).
43. Y. Zhu, L. Dong, C. Wang, K. Hao, J. Wang, L. Zhao, L. Xu, Y. Xia, Q. Jiang, J. Qin, Functional redundancy among Polycomb complexes in maintaining the pluripotent state of embryonic stem cells. *Stem Cell Rep.* **17**, 1198–1214 (2022).
44. K. Wheaton, F. Sarkari, B. Stanly Johns, H. Davarinejad, O. Egorova, L. Kaustov, B. Raught, V. Saridakis, Y. Sheng, UbE2E1/UBCH6 is a critical *in vivo* E2 for the PRC1-catalyzed ubiquitination of H2A at Lys-119. *J. Biol. Chem.* **292**, 2893–2902 (2017).
45. H. Niwa, J. Miyazaki, A. G. Smith, Quantitative expression of Oct-3/4 defines differentiation, dedifferentiation or self-renewal of ES cells. *Nat. Genet.* **24**, 372–376 (2000).
46. J. L. Kopp, B. D. Ormsbee, M. Desler, A. Rizzino, Small increases in the level of Sox2 trigger the differentiation of mouse embryonic stem cells. *Stem Cells* **26**, 903–911 (2008).
47. M. Rape, Ubiquitylation at the crossroads of development and disease. *Nat. Rev. Mol. Cell Biol.* **19**, 59–70 (2018).
48. B.-H. Rhie, A. M. Antao, J. K. Karapurkar, M.-S. Kim, W.-J. Jo, S. Ramakrishna, K.-S. Kim, Ubiquitin-specific protease 3 deubiquitinates and stabilizes Oct4 protein in human embryonic stem cells. *Int. J. Mol. Sci.* **22**, 5584 (2021).
49. X. Wei, J. Guo, Q. Li, Q. Jia, Q. Jing, Y. Li, B. Zhou, J. Chen, S. Gao, X. Zhang, M. Jia, C. Niu, W. Yang, X. Zhi, X. Wang, D. Yu, L. Bai, L. Wang, J. Na, Y. Zou, J. Zhang, S. Zhang, D. Meng, Bach1 regulates self-renewal and impedes mesendodermal differentiation of human embryonic stem cells. *Sci. Adv.* **5**, eaau7887 (2019).
50. M. Beringer, P. Pisano, V. Di Carlo, E. Blanco, P. Chammas, P. Vizan, A. Gutierrez, S. Aranda, B. Payer, M. Wierer, L. Di Croce, EPOP functionally links elongin and Polycomb in pluripotent stem cells. *Mol. Cell* **64**, 645–658 (2016).
51. F. Wang, F. El-Saafin, T. Ye, M. Stierle, L. Negroni, M. Durik, V. Fischer, D. Devys, S. D. Vincent, L. Tora, Histone H2Bub1 deubiquitylation is essential for mouse development, but does not regulate global RNA polymerase II transcription. *Cell Death Differ.* **28**, 2385–2403 (2021).
52. L. Nie, C. Wang, X. Liu, H. Teng, S. Li, M. Huang, X. Feng, G. Pei, Q. Hang, Z. Zhao, B. Gan, L. Ma, J. Chen, USP7 substrates identified by proteomics analysis reveal the specificity of USP7. *Genes Dev.* **36**, 1016–1030 (2022).
53. A. Sijm, Y. Atlasi, J. A. van der Knaap, J. Wolf van der Meer, G. E. Chalkley, K. Bezstarosti, D. H. W. Dekkers, W. A. S. Doff, Z. Ozgur, I. W. F. J. van, J. A. A. Demmers, C. P. Verrijzer, USP7 regulates the ncPRC1 Polycomb axis to stimulate genomic H2AK119ub1 deposition uncoupled from H3K27me3. *Sci. Adv.* **8**, eabq7598 (2022).
54. L. Tavares, E. Dimitrova, D. Oxley, J. Webster, R. Poot, J. Demmers, K. Bezstarosti, S. Taylor, H. Ura, H. Koide, A. Wutz, M. Vidal, S. Elderkin, N. Brockdorff, RYBP-PRC1 complexes mediate H2A ubiquitylation at polycomb target sites independently of PRC2 and H3K27me3. *Cell* **148**, 664–678 (2012).
55. N. R. Rose, H. W. King, N. P. Blackledge, N. A. Fursova, K. J. Ember, R. Fischer, B. M. Kessler, R. J. Klose, RYBP stimulates PRC1 to shape chromatin-based communication between Polycomb repressive complexes. *eLife* **5**, e18591 (2016).
56. N. Kon, Y. Kobayashi, M. Li, C. L. Brooks, T. Ludwig, W. Gu, Inactivation of HAUSP in vivo modulates p53 function. *Oncogene* **29**, 1270–1279 (2010).
57. L. Chen, Q. Tong, X. Chen, P. Jiang, H. Yu, Q. Zhao, L. Sun, C. Liu, B. Gu, Y. Zheng, L. Fei, X. Jiang, W. Li, G. Volpe, M. M. Abdul, G. Guo, J. Zhang, P. Qian, Q. Sun, D. Neculai, M. A. Esteban, C. Li, F. Wen, J. Ji, PHC1 maintains pluripotency by organizing genome-wide chromatin interactions of the *Nanog* locus. *Nat. Commun.* **12**, 2829 (2021).
58. K. Nishimura, T. Fukagawa, H. Takisawa, T. Kakimoto, M. Kanemaki, An auxin-based degron system for the rapid depletion of proteins in nonplant cells. *Nat. Methods* **6**, 917–922 (2009).
59. T. Zhu, Y. Zhu, Y. Xuan, H. Gao, X. Cai, S. R. Piersma, T. V. Pham, T. Schelfhorst, R. Haas, I. V. Bijnsdorp, R. Sun, L. Yue, G. Ruan, Q. Zhang, M. Hu, Y. Zhou, W. J. Van Houdt, T. Y. S. Le Large, J. Cloos, A. Wojtuszkiewicz, D. Koppers-Lalic, F. Bottger, C. Scheepbouwer, R. H. Brakenhoff, G. van Leenders, J. N. M. Ijzermans, J. W. M. Martens, R. D. M. Steenbergen, N. C. Grieken, S. Selvarajan, S. Mantoo, S. S. Lee, S. J. Y. Yeow, S. M. F. Alkaff, N. Xiang, Y. Sun, X. Yi, S. Dai, W. Liu, T. Lu, Z. Wu, X. Liang, M. Wang, Y. Shao, X. Zheng, K. Xu, Q. Yang, Y. Meng, C. Lu, J. Zhu, J. Zheng, B. Wang, S. Lou, Y. Dai, C. Xu, C. Yu, H. Ying, T. K. Lim, J. Wu, X. Gao, Z. Luan, X. Teng, P. Wu, S. Huang, Z. Tao, N. G. Iyer, S. Zhou, W. Shao, H. Lam, D. Ma, J. Ji, O. L. Kon, S. Zheng, R. Aebersold, C. R. Jimenez, T. Guo, DPHL: A DIA pan-human protein mass spectrometry library for robust biomarker discovery. *Genomics Proteomics Bioinformatics* **18**, 104–119 (2020).
60. D. Szklarczyk, A. L. Gable, K. C. Nastou, D. Lyon, R. Kirsch, S. Pyysalo, N. T. Doncheva, M. Legeay, T. Fang, P. Bork, L. J. Jensen, C. von Mering, The STRING database in 2021: Customizable protein-protein networks, and functional characterization of user-uploaded gene/measurement sets. *Nucleic Acids Res.* **49**, D605–D612 (2021).
61. S. Chen, Y. Zhou, Y. Chen, J. Gu, Fastp: An ultra-fast all-in-one FASTQ preprocessor. *Bioinformatics* **34**, i884–i890 (2018).
62. D. Kim, B. Langmead, S. L. Salzberg, HISAT: A fast spliced aligner with low memory requirements. *Nat. Methods* **12**, 357–360 (2015).

63. M. I. Love, W. Huber, S. Anders, Moderated estimation of fold change and dispersion for RNA-seq data with DESeq2. *Genome Biol.* **15**, 550 (2014).
64. B. Langmead, S. L. Salzberg, Fast gapped-read alignment with Bowtie 2. *Nat. Methods* **9**, 357–359 (2012).
65. J. Feng, T. Liu, B. Qin, Y. Zhang, X. S. Liu, Identifying ChIP-seq enrichment using MACS. *Nat. Protoc.* **7**, 1728–1740 (2012).
66. H. Thorvaldsdottir, J. T. Robinson, J. P. Mesirov, Integrative genomics viewer (IGV): High-performance genomics data visualization and exploration. *Brief. Bioinform.* **14**, 178–192 (2013).
67. F. Ramirez, D. P. Ryan, B. Gruning, V. Bhardwaj, F. Kilpert, A. S. Richter, S. Heyne, F. Dundar, T. Manke, deepTools2: A next generation web server for deep-sequencing data analysis. *Nucleic Acids Res.* **44**, W160–W165 (2016).
68. A. R. Quinlan, I. M. Hall, BEDTools: A flexible suite of utilities for comparing genomic features. *Bioinformatics* **26**, 841–842 (2010).
69. M. P. Meers, D. Tenenbaum, S. Henikoff, Peak calling by sparse enrichment analysis for CUT&RUN chromatin profiling. *Epigenetics Chromatin* **12**, 42 (2019).

Acknowledgments: We thank Q. Sun and D. Neculai at Department of Biochemistry and Department of Cell Biology, Zhejiang University School of Medicine for advice on the project, respectively. **Funding:** This work was supported by grants from the National Natural Science Foundation of China (32170795, 91849131, and 32200659), Zhejiang Province Natural Science Foundation (LZ21C120001), and The Construction Fund of Key Medical Disciplines of Hangzhou (no. OO20200055). **Author contributions:** Conceptualization: J.J. Experimental design: J.J., T.G., and Y.Z. Performing experiments: C.Liu, L.S., Y.T., Q.W., C.Li, T.L., N.Y., Y.X., and X.Y. Data analysis: C.Liu, L.S., Q.W., Y.X., and Y.Z. Funding acquisition: J.J. and T.G. Writing—original draft: J.J. and C.Liu. Writing—review and editing: J.J. **Competing interests:** T.G. and Y.Z. are shareholders of Westlake Omics Inc. All other authors declare that they have no competing interests. **Data and materials availability:** All data needed to evaluate the conclusions in the paper are present in the paper and/or the Supplementary Materials. RNA-seq and CUT&Tag data are available in the GEO database with the accession number GSE197427 and GSE197157, respectively. The accession numbers of previously published ChIP-seq data for SOX2 and RYBP are GSE56312 and GSE136584, respectively. MS data are available via ProteomeXchange with accession number PXD039633. All codes used in this study for bioinformatics are freely available with the link https://github.com/DrLyo/USP7-represses-lineage-differentiation-of-mESCs or Dryad at https://doi.org/10.5061/dryad.hx3ffbgk5. All other data supporting the findings of this study are available through the repositories mentioned in this statement.

Submitted 14 August 2022
Accepted 12 April 2023
Published 17 May 2023
10.1126/sciadv.ade3888